nature portfolio

Peer Review File

Bioinspired Gel Polymer Electrolyte for Wide Temperature Lithium Metal Battery

Corresponding Author: Professor Shenmin Zhu

This file contains all reviewer reports in order by version, followed by all author rebuttals in order by version.

Version 0:

Reviewer comments:

Reviewer #1

(Remarks to the Author)
Title: Bioinspired Topological Polymer Electrolyte for Ultra-Wide Temperature Lithium Metal Battery

For the development of wide-temperature lithium metal batteries with polymer electrolytes, this paper introduces topological polymer electrolytes, composed of PTFMA as the polymer skeleton, FEP as the coupling additive, PEGDA as the cross-linker, along with FEC and LiTFSI. The authors hypothesize that the side chains of PTFMA can interact with FEP through double dipole coupling, and this intermolecular interaction may weaken the coordination of Li+ ions, resulting in a weak solvation structure. To validate the hypothesis of weakly-solvated topological polymer electrolytes (WSPE), the authors systematically investigated the static and dynamic properties of WSPE using various experimental methods (FTIR, EIS, & TEM), along with theoretical MD simulations. The optimized WSPE demonstrates high ionic conductivity, a high Li+ transfer number, and a broad electrochemical window. In addition, the WSPE-based Li/Li, NCM/Li, and pouch cells show better electrochemical, cycling, and rate performances, compared to liquid electrolyte-based cells. These results could be valuable for readers interested in the development of new polymer electrolytes for wide-temperature range Li metal batteries. However, the description of the bioinspired topological polymer electrolyte, shown in Figure 1d, is not clear to this reviewer, as there is no evidence provided regarding morphological properties. Additionally, there still exists several questionable points that need to be addressed before this paper can be published, detail below.

1. To validate the weak solvation structure of WSPE and demonstrate its outstanding electrochemical performance, the authors conducted comparison experiments between WSPE and a liquid electrolyte. However, to further substantiate this hypothesis (double dipole coupling), it would be beneficial to investigate the effect of FEP on the solvation structure, interface stability, and electrochemical performance. This might be achieved by comparing the results obtained from FEP-free polymer electrolytes with those from WSPE.

2. On page 3, Line 6: The manuscript contains some typographical errors, such as “blow”. The authors should carefully review both the text and figures to correct such mistakes and ensure the document’s accuracy.

3. On page 6, Line 8: The authors conducted the DFT calculation between components in WSPE to investigate the binding energy, as listed in Table S1. However, the calculated energy values seem to be unusually high. Thus, it would be helpful to provide detailed information on the binding energy calculation, including the specific calculation formula used.

4. On page 7, line 7-13, Figures 2d & 2e: In Figure 2, the authors presented the coordination number of Li+ with TFSI, FEC, FEP, and PTFMA in WSPE. However, the solvation structure and coordination number (CN) of Li+ in liquid electrolytes were not discussed. Specifically, does the interaction between Li+ cation and FEP in liquid electrolytes become stronger, potentially increasing the CN of Li+ with FEP? Or does TFSI- maintain a higher CN due to its role as the counterion for Li+? Again, the authors should compare the simulation results of the solvation structure with and without FEC to confirm that WSPE functions as a weakly-solvated topological polymer electrolyte. This comparison would provide a clearer understanding of how the solvation structures differ between WSPE and liquid electrolytes.

5. On page 7, line 18-20, Figure 2f: The authors mentioned that “The presence of a large number of CIPs minimizes solvent polarization and keeps the FEP away from the electrode to prevent side reactions.” However, this sentence is not clear to this reviewer. Could the authors further explain why a higher CIP number would cause FEP to stay away from the electrode?

6. On page 7, line 27-30, Figures 2g and 2h: The authors discussed the diffusion coefficients of Li+, TFSI-, and FEP, obtained from the MD simulation, noting that FEP exhibits a higher diffusion coefficient than the two ions. This raises the question of why FEP, interacting with PTFMA through double dipole coupling, has a higher diffusion coefficient. Does this imply that FEP can fast move to the electrode? If so, this interpretation seems inconsistent with the FTIR results. Furthermore, the diffusion coefficient of Li+ is similar to one of TFSI-. This may be another case that is contradictory to the high lithium transference number (0.83). Could the authors clarify how similar diffusion coefficients between Li+ and TFSI- contribute to a high lithium transference number?

7. On page 8, Figure 3f: The authors present the cell performances at RT, LT, and HT. However, the LT cycling performance was conducted only at a low C-rate (0.2 C). Is there a specific reason for this?

8. On page 9, line 11-16, Figures S13 and S14: Figures S13 and S14 show the EIS results of liquid electrolyte (LE) and WSPE at different temperatures. It would be helpful to include the equivalent circuit and a table of Rct and RSEI values in SI. To demonstrate that the lower resistance of WSPE after cycling, compared to the liquid electrolyte, is due to the stable EEI generation, it would be beneficial for the authors to provide the interfacial resistance of both WSPE and LE before cycling.

9. On page 10, Line 8: The authors successfully implemented a pouch cell using a high mass loading (23.4 mg/cm2) cathode and a thin Li foil anode with a thickness of 50 μm. Given that the N/P ratio of the pouch cell is expected to be low, it is recommended that the authors provide the N/P ratio value in the manuscript for clarity.

10. On page 10, Line 22, Figure 5a: The authors mentioned that the cell is stable when applied with various current densities up to 1 mA/cm-2. However, in Figure 5a, the specific current densities applied to the cell are not clearly indicated. Please provide detailed information on the range of current densities that was applied to the cell in the figure.

Reviewer #2

(Remarks to the Author)
This paper does not make sense to me, and I suggest its rejection. This would be a unique set-up, having so very low dependence on temperature. This is not consistent with any other observations on solid polymer electrolytes, and barely with liquid electrolytes. The authors have no reasonable explanation for this observation, if it in fact exists. Then, it is not a polymer electrolyte – it is basically a liquid FEC/FEP electrolyte (heavily fluorinated), contained in a polymer matrix. It is clearly a gel, but the entire discussion is written in the context of it being solid polymer electrolyte. If compared with heavily fluorinated liquid electrolytes, the results are not really that impressive. The gel electrolyte contains many components, but is poorly described in terms of composition and preparation.

Then, the entire analogy with a biological system is misleading. I would assume it is an analogy also, rather than an inspiration. This analogy is however just confusing for the reader, and likely incorrect if the true modes of structural organization and ionic transport would be determined.

Reviewer #3

(Remarks to the Author)
Liu et al. demonstrated a functional polymer electrolyte with a concept of weakly solvation structure. Benefitting from its special structure, it shows promising behaviors over a wide temperature range. However, there is some concerns needs to be resolved prior to its publication.

1. The concept of weakly solvating liquid electrolyte now becomes common, while the weakly polymer electrolyte still seems fancy. The question is how to define the concept of weakly-solvated polymer electrolyte? What is superiority over the liquid electrolyte?
2. The polymer electrolyte is initiated by a polymerization process. I have a significant concerns on the liquid residue within the polymer? The amount of liquid residue could considerably strength the ionic transfer and interface stability, however not belongs to the definition of polymer electrolyte. Please clarify the issues.
3. How about the ionic transport mechanism in the polymer electrolyte? The unique transfer mechanism is suggested to compare with the classic PEO and PVDF polymer electrolyte.
4. Continue to the last question, how about the ion diffusion mechanism within the cathode, especially with thick cathode?
5. Despite the beauty of figure drawing, I have some concerns on the scientific aspects on this work. Lots of important electrochemical issues has been neglected, such as the cathode loading, the galvanic discharge/charge protocol (with the cutoff conditions). Some important parameters are suggested to added into the figures, but not just simply listing the rate of 1C, 2C. The cycling rate has no any meaning if there is no other parameters. Same to Figure 5a without no any information about its current density and areal capacity.
6. What is the reason for the fire resistance shown in Figure 1g? The polymer electrolyte seems also flame until its fully collapsed. Is it due to the combustion of residue liquid electrolyte within the polymer electrolyte?
7. Will this solvation structure change under extreme temperatures? Does the desolvation process differ at various temperatures?
8. Lots of supplementary details needs to be provided on the large pouch cell, especially 5 Ah pouch cell, for instance,

picture before and after assembly, digital picture of assembly process, the pouch cell after cycling. I have a huge concerns on the assembly of such high areal high capacity pouch cell, in comparison with liquid electrolytes.

Version 1:

Reviewer comments:

Reviewer #1

(Remarks to the Author)
The authors have thoroughly addressed this reviewer's concerns, and the manuscript has been significantly improved as a result. I now recommend its acceptance without further revision.

Reviewer #3

(Remarks to the Author)
I am satisfied with the response letter and the revised manuscript. I have no further concerns.

Reviewer #4

(Remarks to the Author)
The manuscript entitled "Bioinspired topological polymer electrolyte for ultra-wide temperature lithium metal battery" co-authored by Shuohan Liu, Wensheng Tian, Jieqing Shen, Zhikai Wang, Hui Pan, Xuchen Kuang, Cheng Yang, Shunwei Chen, Xiujun Han, Hengdao Quan, and Shenmin Zhu presents an interesting study on a 1 M LiTFSI FEP + 5 wt% FEC embedded in a PTFMA matrix electrolyte. The originality of this manuscript lies in the selection of FEP and PTFMA which present an asymmetrical structure that induces double dipole interaction. This unique configuration seems to form a weak solvation structure that offers fast and uniform Li+ deposition and stable electrolyte-electrode interfaces at extreme temperatures. Remarkable performances are demonstrated. However, the present revised manuscript lack in explaining the intrinsic reason and mechanism leading to such remarkable performances. Furthermore, this manuscript defines the WSPE as a separate category from GPE. However, this material being a liquid electrolyte (LE) trapped in a polymer matrix is in fact a GPE, so it is better not to create an unnecessary category. In addition, the analogy with Elodea densa is not helpful for reader and rather confusing. The is the main misleading point as this algae is as a solid-like structure in water whereas the design material is a fluorinated gel electrolyte not a solid. Indeed, no mechanical/viscosity characterization are provided. Thanks to the originality but due to lack of clearness in the discussion, we recommend this manuscript to be accepted but after some major changes.
We have couple of comments thus to address as listed below:

1. The comparison with the algae would make sense if the polymer matrix would stretch like the leaves in water which is useless for the present work. In addition, other publications already exists for GPE with branched polymer matrix. (e.g. https://doi.org/10.1016/j.ssi.2016.05.019)
2. A GPE is a LE embedded in a polymer matrix. From the experimental section it seems that the electrolyte composition is about 65 wt.% of solvent (FEC + FEP) and the rest is LiTFSI salt 13.5 wt.%, PTFMA polymer 20 wt.%, crosslinker 1wt.%, and initiator 0.5 wt.%. Therefore, the electrolyte is a GPE not a new class of electrolyte. Please adjust the manuscript title and text accordingly. A proposition : weakly solvated gel polymer electrolyte (WSGPE).
3. How does the PEGDA interact with the polymer matrix? Is there any remaining PEGDA in the system ?
4. Page 3 line 8 is grammatically wrong.
5. Previous work on PTFMA should be cited: https://doi.org/10.1016/j.jpowsour.2024.235189 doi/abs/10.1002/cnma.202400180, https://doi.org/10.1002/eem2.12351.
6. Previous work of FEP should be cited: https://www.nature.com/articles/s41467-023-36853-x.
7. There is not much explanation on the effect of FEC which is unclear in the text. So, does the materials behave the same without FEC in iis formulation. What is the corresponding volume fraction? What about diffusivity of FEC and the possibility to coordinate cation or anion and participate in the ionic transport ? This could explain the high conductivity even at low temperature. In addition, is there degradation of FEC with Li metal to promote a stable SEI ? In short, it is important to decorrelate the effect of FEC from the gel electrolyte.
8. Regarding FTIR discussion on Page 7: the reference sited in the manuscript employ Raman not FTIR to discuss presence of FA, CIP, and AGG.
9. "The results from the analysis of FTIR and NMR indicate that only when FEP and PTFMA coexist, a weak solvation structure dominated by anions can be achieved (Supplementary Figs. 7-9)." However, a small but visible NMR shift from FEC based LE to FEC filled PTFMA is also observed, which indicates that a weaker solvation structure dominated by anions is formed. However, the shift is stronger for FEP probably due to the mirrored structure of PTFMA and FEP. Please rephrase.
10. The electrochemical stability window seems incorrect. In figure S10 there is an oxidation wave starting at about 4.8 V. Please revised.
11. Impedance spectroscopy in Nyquist representation must be orthonormal. Please correct all the EIS graph.
12. Tafel plot are provided but from which type experiments and electrochemical cell ? Where are the raw data to make such plots ?
13. "The uniform and thin CEI not only reduces the polarization during the cycling, but also restrains the structure transition

of NCM811." Can you confirm this observation by XRD? Because HRTEM is a local measurement while XRD would give you a more concreate idea of the whole instability if any.
14. "The wide electrochemical window, high ionic conductivity, and Li+ transference number make the WSPE can be used in high-voltage Li metal batteries." This sentence is grammatically wrong. Please rephrase.
15. Regarding TOF-SIMS, Why depth scale is missing? How about other elements?
16. Please indicate the pressure applied during cycling if any.
17. Method parts: only FTIR and some electrochemical methods are provided whereas plenty of techniques are reported in this work from Raman to TOF-SIM via NMR etc.. This is not consistent. How were samples prepared for XPS and TOF-SIMS characterizations.
18. The reviewer spent most of their time reding the supporting info file (33 figures in it) rather than focusing on the manuscript which presents rather concept figures than experimental data.

Reviewer #5

(Remarks to the Author)
I co-reviewed this manuscript with one of the reviewers who provided the listed reports. This is part of the Nature Communications initiative to facilitate training in peer review and to provide appropriate recognition for Early Career Researchers who co-review manuscripts.

Version 2:

Reviewer comments:

Reviewer #4

(Remarks to the Author)
After careful reading of the responses from the authors and of the revised manuscript, I believe that the manuscript is worth to be published in Nature Communication.

Reviewer #5

(Remarks to the Author)
I co-reviewed this manuscript with one of the reviewers who provided the listed reports. This is part of the Nature Communications initiative to facilitate training in peer review and to provide appropriate recognition for Early Career Researchers who co-review manuscripts.

Response to Reviewer #1:

1. For the development of wide-temperature lithium metal batteries with polymer electrolytes, this paper introduces topological polymer electrolytes, composed of PTFMA as the polymer framework, FEP as the coupling additive, PEGDA as the cross-linker, along with FEC and LiTFSI. The authors hypothesize that the side chains of PTFMA can interact with FEP through double dipole coupling, and this intermolecular interaction may weaken the coordination of Li^+ ions, resulting in a weak solvation structure. To validate the hypothesis of weakly-solvated topological polymer electrolytes (WSPE), the authors systematically investigated the static and dynamic properties of WSPE using various experimental methods (FTIR, EIS, & TEM), along with theoretical MD simulations. The optimized WSPE demonstrates high ionic conductivity, a high Li^+ transfer number, and a broad electrochemical window. In addition, the WSPE-based Li/Li, NCM/Li, and pouch cells show better electrochemical, cycling, and rate performances, compared to liquid electrolyte-based cells. These results could be valuable for readers interested in the development of new polymer electrolytes for wide-temperature range Li metal batteries. However, the description of the bioinspired topological polymer electrolyte, shown in Figure 1d, is not clear to this reviewer, as there is no evidence provided regarding morphological properties. Additionally, there still exists several questionable points that need to be addressed before this paper can be published, detail below.

Response: Thank you for your kind comments.

To clearly present our design concept, we have updated Fig. 1 in the revised manuscript (see Fig. R1 below). The inspiration from water grass (*Elodea densa*) stems from the integration of its structure and function, which have evolved over billions of years to adapt to environmental challenges. *Elodea densa* has a unique structure that allows water to pass smoothly and maintains its structural integrity through the rapid swinging of short lateral blades against strong currents. Meanwhile, the epidermal cell walls of *Elodea densa* are composed of hydrophilic polysaccharides which enhance the interaction of the blades with the water. This dynamic interaction forces *Elodea densa* to exhibit a stretched state in the water and doesn't impede water transport.

Inspired by the structure-function integration of *Elodea densa*, we designed a

brush-like polymer with short side chains to reduce the transport resistance of Li^+ solvation clusters under current. Importantly, a Li^+ solvation cluster is constructed that allows it to form unique dynamic non-bonding interactions with the short side chains of polymer brushes, which mimick the dynamic interactions of *Elodea densa* with water. The strong interaction between the polymer framework and the coupling agent not only ensures the stretching of the polymer chains, but also effectively induces a weak solvation structure (Fig. R1d). TFMA monomer was used for in situ polymerization to form a brush-like PTFMA framework, and FEP was coupled with the side chain of PTFMA. This double dipole coupling interaction successfully induced the generation of the weak solvation structure (Fig. R1e). Therefore, both high ion conductivity and easy desolvation would be achieved simultaneously, and the operation temperature range can be expanded. The above discussion has been added in the manuscript to strengthen the description of our concept (Paragraph 1, Page 5).

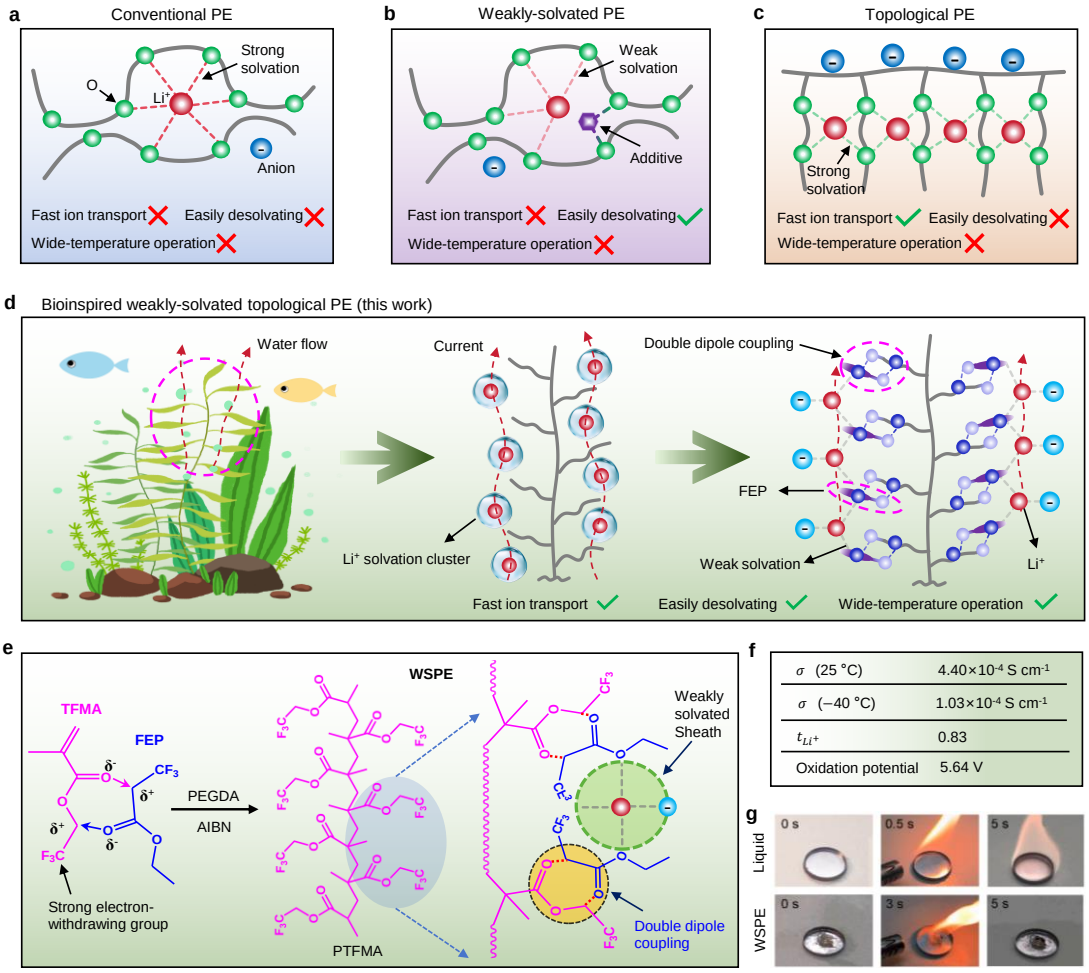

Fig. R1 Material design, fabrication, and properties of bioinspired weakly-solvated topological PE (Fig. 1 in revised manuscript)**.** (**a**) Conventional PE. (**b**)

Weakly-solvated PE. (**c**) Topological PE. (**d**) Bioinspired weakly-solvated topological PE. (**e**) Structures and fabrication method of WSPE. (**f**) Electrochemical properties of WSPE. (**g**) Flame-retardant performance of WSPE.

To further validate the rationality of our concept, we conducted MD simulation. As shown in Fig. R2, the polymer PTFMA in this work has a brush-like configuration which is similar to that of *Elodea densa*. Meanwhile, the FEP molecules are inclined to accumulate around the polymer chains by a relatively high binding energy calculated by DFT (Table R1, Supplementary Table 1 in Supplementary information). As a result, the coupled structure of the FEP and PTFMA side chains regulate the solvation structure of the electrolyte for ultra-wide temperature lithium metal battery, showing the structure-function integration similar to *Elodea densa.* Fig. R2 has also been added in the revised Supplementary information as Supplementary Fig. 1.

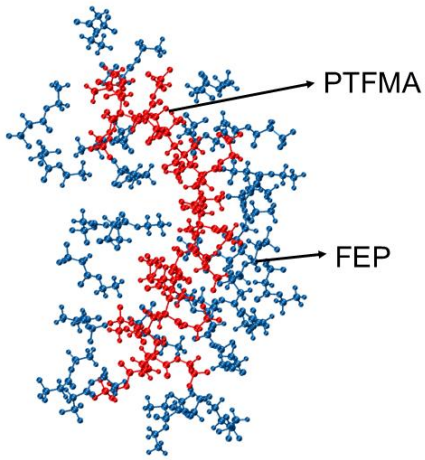

Fig. R2 (Supplementary Fig. 1 in revised Supplementary information). Snapshots of WSPE partial MD simulations.

Table R1. Binding energy between components in WSPE calculated by DFT.

Component A	Component B	Binding energy (kJ/mol)
$TFSI^-$	FEC	2727.87
$TFSI^-$	FEP	15645.06
$TFSI^-$	PTFMA	3346.05
PTFMA	FEC	7975.83
PTFMA	FEP	29380.90

2. To validate the weak solvation structure of WSPE and demonstrate its outstanding electrochemical performance, the authors conducted comparison experiments between WSPE and a liquid electrolyte. However, to further substantiate this hypothesis (double dipole coupling), it would be beneficial to investigate the effect of FEP on the solvation structure, interface stability, and electrochemical performance. This might be achieved by comparing the results obtained from FEP-free polymer electrolytes with those from WSPE.

Response: Thank you very much for your suggestion.

As you mentioned, the addition of FEP-free polymer electrolyte as a comparison is necessary to further substantiate the existence of double dipole coupling between FEP and the PTFMA framework. In order to ensure that the ratio of liquid and polymer components in the comparison samples is consistent with that of WSPE, we replaced FEP in WSPE with an equal amount of FEC to obtain a FEP-free polymer electrolyte (denoted as FEP-free PE). Furthermore, we have supplemented another control sample, namely PTFMA-free polymer electrolyte (PTFMA-free PE), which was prepared by replacing TFMA in the WSPE precursor with an equal amount of poly(ethylene glycol) diacrylate (PEGDA). We have conducted these two control experiments and the results including the effects of interaction between FEP and PTFMA on the solvation structure, interface stability and electrochemical performance are as follows:

(1) The effect on solvation structure

As shown in Fig. R3a, the precursor of FEP-free PE shows a distinct peak of C=C bond at 1640 cm^{-1}. After curing at 70 °C for 5 h, the C=C peak disappears obviously, indicating the complete polymerization of TFMA. The peak of the S−N−S stretching vibration of $TFSI^-$ is shown in Fig. R3b, from which can study the solvation structure

of electrolytes. $TFSI^-$ in the FEC liquid electrolyte (1 M LiTFSI in FEC) mainly exists in the form of free anions (FAs), and the addition of TFMA precursors has no distinct effect on the solvation structure of the FEC liquid electrolyte. $TFSI^-$ anions in FEP-free PE are also dominated by FAs. These results indicate that the PTFMA framework has no significant effect on the solvation structure of the FEC liquid electrolyte. These results have been added in the revised Supplementary information as Supplementary Fig. 7.

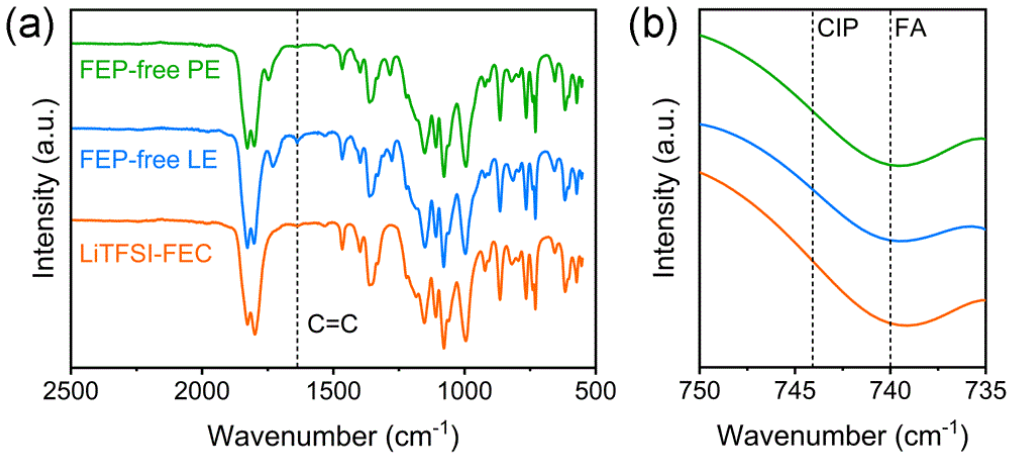

Fig. R3 (Supplementary Fig. 7 in revised Supplementary information). (a) FTIR spectra and (b) S−N−S stretching of $TFSI^-$ of FEC liquid electrolyte, FEP-free LE and FEP-free PE, respectively.

The FTIR spectra of the liquid electrolyte (1M LiTFSI in FEP with 5 wt% FEC), PTFMA-free PE and WSPE are compared in Fig. R4. There is no visible difference between the solvation structures of the liquid electrolyte and the PTFMA-free PE, both dominated by FAs without ion aggregates (AGGs). That means there is no measurable interaction between the FEP and PEGDA framework, and PEGDA is not able to induce the formation of weak solvation structure. In contrast, the peak of $TFSI^-$ in WSPE shows a significant blue shift, indicating that PTFMA could induce the solvation structure transition from FAs-dominated to contact ion pairs (CIPs)-dominated state. In a word, the weak solvation structure can be induced by the double dipole coupling interaction when the FEP and PTFMA coexist. These results have been added in the revised Supplementary information as Supplementary Fig. 8.

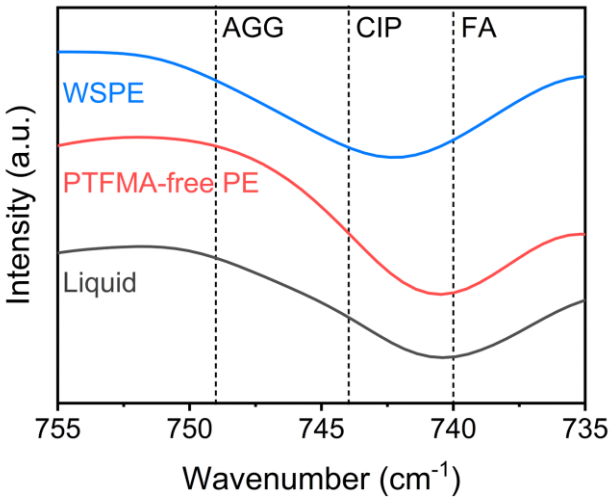

Fig. R4 (Supplementary Fig. 8 in revised Supplementary information). FTIR spectra of liquid electrolyte, PTFMA-free PE and WSPE.

(2) The effect on interface stability

In order to reveal the effect of interaction between FEP and PTFMA on the interface stability, Li symmetric cells were assembled by using WSPE, liquid electrolyte, FEP-free PE and PTFMA-free PE, respectively. The cells were cycled at 0.5 mA cm^{-2} and 0.5 mAh cm^{-2} and the results are demonstrated in Fig. R5. The electrochemical impedance spectroscopy (EIS) during cycling were used to reflect the stability of the electrolyte to Li metal. The Li/WSPE/Li cell can be stably cycled at room temperature for more than 1500 h without short-circuiting (Fig. R5a). With the cycling, the interfacial impedance of the Li/WSPE/Li cell decreased continuously (Fig. R5e), then stabilized at about 120 Ω after 100 cycles, indicating the formation of a stable high conductivity SEI layer. As a contrast, the cells based on liquid electrolyte, FEP-free PE and PTFMA-free PE were short-circuited at 166 h, 293 h and 236 h, respectively (Figs. R5b-d). During cycling, the interfacial impedance of all the three samples decreased first and then increased before short circuit (Figs. R5f-h). This indicates that the generated SEI layer is unstable and cannot effectively inhibit the decomposition of the electrolyte, and the uneven Li deposition leads to the rapid growth of dendrites until it penetrates the separator and short circuits.

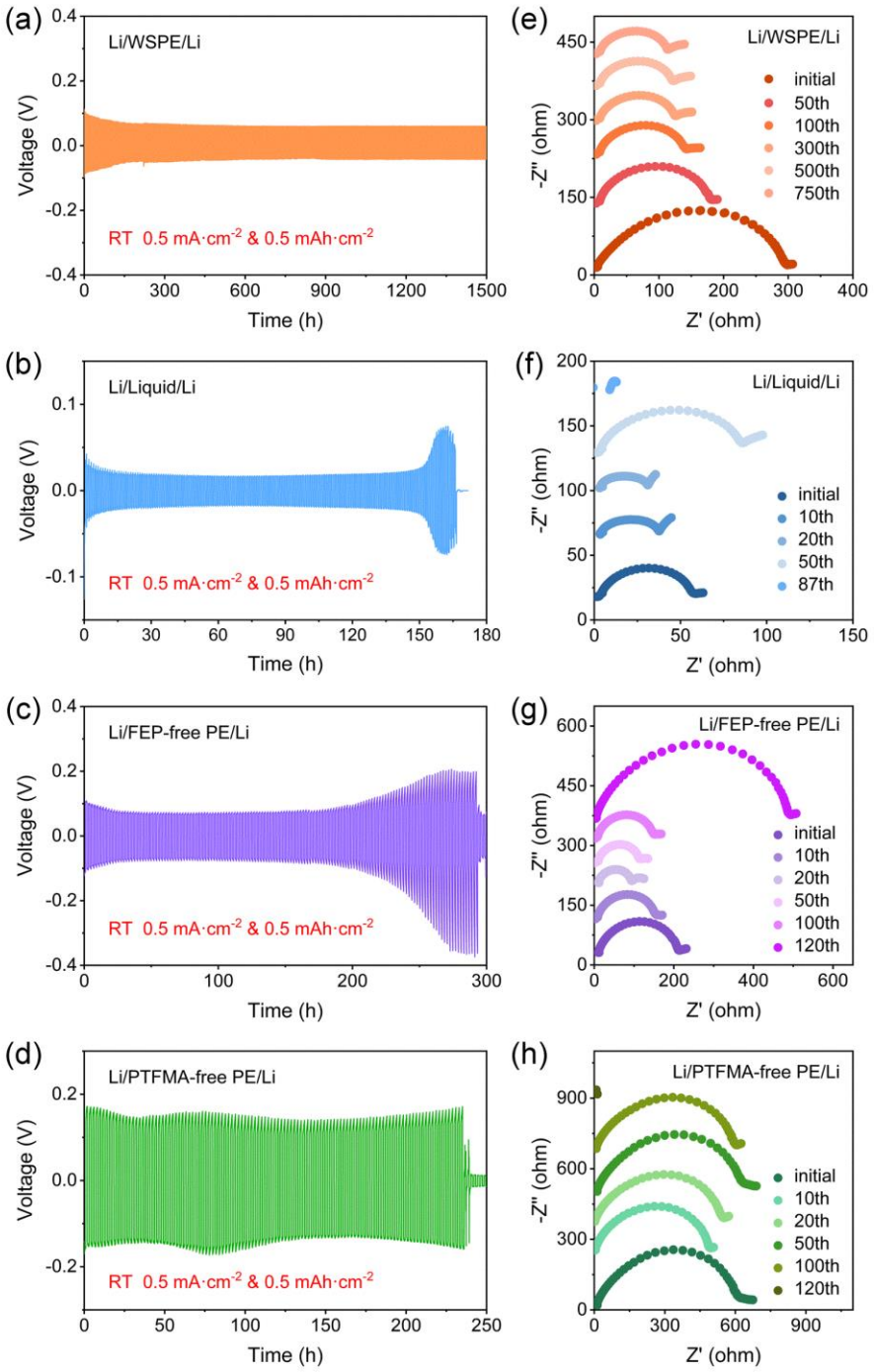

Fig. R5 (Supplementary Figs. 30 and 31 in revised Supplementary information). Galvanostatic cycling performance of Li symmetric cells using (a) WSPE, (b) liquid electrolyte, (c) FEP-free PE and (d) PTFMA-free PE. EIS plots during cycling of Li symmetric cells using (e) WSPE, (f) liquid electrolyte, (g) FEP-free PE and (h) PTFMA-free PE.

The SEM images of the Li surfaces after cycling give strong evidence to support

the above results (Fig. R6). Even after long-term cycling (Fig. R6a), the Li surface of the Li/WSPE/Li cell remains overall dense and smooth, with no porous structure or Li dendrites. In contrast, the surfaces of Li anodes from liquid electrolyte, FEP-free LE and PTFMA-free PE systems show obvious dendritic morphologies (Figs. R6b-d), resulting from the short-circuit and severe capacity fading. It is reasonable to conclude that the unique double dipole coupling interaction between FEP and PTFMA effectively induces the generation of the stable interfacial phase. These results have been added in the revised Supplementary information as Supplementary Figs. 30-32 and corresponding discussion has been added in the revised manuscript (Paragraph 3, Page 12).

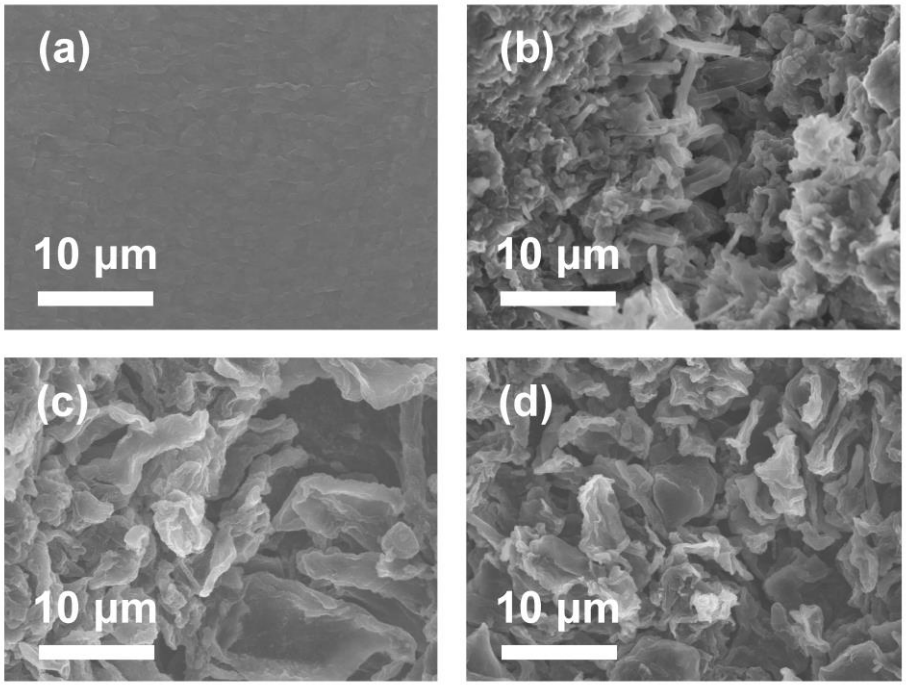

Fig. R6 (Supplementary Fig. 32 in revised Supplementary information). SEM images of Li surfaces after cycling from (a) Li/WSPE/Li, (b) Li/Liquid/Li, (c) Li/FEP-free PE/Li and (d) Li/PTFMA-free PE/Li cells after cycling.

(3) The effect on electrochemical performance

The cycling performance of Li/NCM811 cells assembled with different electrolytes at 1C is conducted, as shown in Fig. R7. The Li/WSPE/NCM811 cell exhibits the most excellent cycling stability, delivering a capacity of 120.8 mAh g^{-1} after 300 cycles, with an average capacity decay of only 0.087% per cycle. For the controlled cells using liquid electrolyte and FEP-free PE, initial capacities of 167.8

mAh g^{-1} and 169.3 mAh g^{-1} are measured, respectively. However, after 300 cycles, the capacities decrease to only 51.4% and 50.5% of their initial values for the cells based on liquid electrolyte and FEP-free PE, respectively. Similarly, the Li/PTFMA-free PE/NCM811 cell only delivers a capacity of 63.2 mAh g^{-1} after 300 cycles, which is 43.3% of the initial capacity. The above results illustrate that the unique structure and interactions in WSPE endow it with outstanding high-voltage cycling stability. These results have been added in the revised Supplementary information as Supplementary Fig. 13.

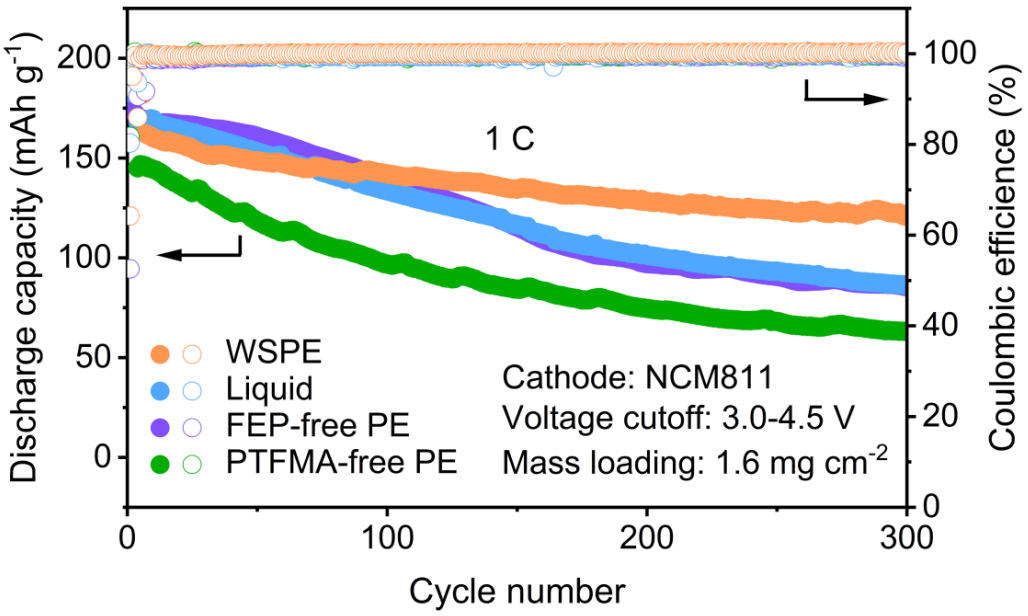

Fig. R7 (Supplementary Fig. 13 in revised Supplementary information). Cycling performance of Li/NCM811 cells using different electrolytes at 1C between 3−4.5 V.

The comparisons above reveal the effect of the interaction between FEP and PTFMA on the solvation structure, interface stability, and electrochemical performance. Only when FEP and PTFMA are simultaneously present, a weak solvation structure dominated by CIPs can be achieved, leading to excellent interface stability and electrochemical performance.

3. On page 3, Line 6: The manuscript contains some typographical errors, such as “blow”. The authors should carefully review both the text and figures to correct such mistakes and ensure the document’s accuracy.

Response: We have checked carefully both the text and figures to avoid narrative ambiguities, possible errors and misspellings. The errors have been corrected and yellow highlighted in our revised manuscript.

4. On page 6, Line 8: The authors conducted the DFT calculation between components in WSPE to investigate the binding energy, as listed in Table S1. However, the calculated energy values seem to be unusually high. Thus, it would be helpful to provide detailed information on the binding energy calculation, including the specific calculation formula used.

Response: Thank you very much for your valuable comments.

The detailed information of the interaction energy calculation is as follows: During calculations, the non-bonding intermolecular interaction is composed of the Van der Waals interaction and the Coulomb interaction. The Van der Waals interaction can further be divided into the short-ranged part, $E_{\text{vdw-SR}}$, in the cut-off distance and the long-ranged part, $E_{\text{Disper-corr.}}$, due to the correction of dispersion. When using Particle-Mesh-Ewald (PME) algorithm to handle the electrostatic interaction, the coulomb interaction can be further divided into the short-ranged part, $E_{\text{Coul-SR}}$, in the real space and the long-ranged part, $E_{\text{Coul-recip.}}$, in the reciprocal space.

When the interaction energy between molecular A and molecular B, ΔE(A-B), is calculated, the following steps are performed. Firstly, the trajectory for the partial system, which contains both molecules A and B, $Traj_{\text{AB}}$, is extracted from the dynamical trajectory for the whole system, which contains all types of molecules and ions. And then the separate trajectory of molecules A, $Traj_{\text{A}}$, and molecules B, $Traj_{\text{B}}$, are extracted from the total one, respectively. Secondly, the molecular dynamics simulation is rerun according to each trajectory. And the four parts of energies, namely, $E_{\text{vdw-SR}}$, $E_{\text{Disper-corr.}}$, $E_{\text{Coul-SR}}$ and $E_{\text{Coul-recip.}}$, are recorded for statistics. The energies E(AB), E(A), E(B) can be obtained as the summation of their respective four energies. Finally, ΔE(A-B) is calculated as $\Delta E(\text{A-B}) = E(\text{AB})-E(\text{A})-E(\text{B})$.

The results are presented in Tables R2-R6.

Table R2. The related energies in calculating the interaction energy between $TFSI^-$ anion and FEC molecule, $\Delta E(TFSI^-\text{-FEC}) = -2727.869$ (kJ/mol)

Energy (kJ/mol)		$E(TFSI^-+FEC)$	$E(TFSI^-)$	E(FEC)
vdw part	LJ(SR)	−18647.9	−10178	−3132.98
	Disper. corr.	−895.273	−294.523	−161.221
Coulomb part	Coul. (SR)	−7026.31	10800.7	−19286.8
	Coul. recip.	141529	136581	3359.21
Summation		114959.517	136909.177	−19221.791

Table R3. The related energies in calculating the interaction energy between $TFSI^-$ anion and FEP molecule, $\Delta E(TFSI^-\text{-FEP}) = -15645.057$ (kJ/mol)

Energy (kJ/mol)		$E(TFSI^-+FEP)$	$E(TFSI^-)$	E(FEP)
vdw part	LJ(SR)	−95380.4	−10178	−59369.7
	Disper. corr.	−6201.6	−294.523	−3784.96
coulomb part	Coulomb (SR)	168962	10800.7	150710
	Coul. recip.	146113	136581	4673.54
Summation		213493	136909.177	92228.88

Table R4. The related energies in calculating the interaction energy between $TFSI^-$ anion and PTFMA molecule, $\Delta E(TFSI^-\text{-PTFMA}) = -3346.049$ (kJ/mol)

Energy (kJ/mol)		$E(TFSI^-+PTFMA)$	$E(TFSI^-)$	E(PTFMA)
vdw part	LJ(SR)	−21220.6	−10178	−7721.06
	Disper. corr.	−1504.29	−294.523	−464.838
coulomb part	Coulomb (SR)	−92834.6	10800.7	−103970
	Coul. recip.	138140	136581	1173.28
Summation		22580.51	136909.177	−110982.618

Table R5. The related energies in calculating the interaction energy between PTFMA and FEC molecule, ΔE(PTFMA-FEC) = −7975.831 (kJ/mol)

Energy (kJ/mol)		*E*(PTFMA+FEC)	*E*(PTFMA)	*E*(FEC)
vdw part	LJ(SR)	−16860.2	−7721.06	−3132.98
	Disper. corr.	−1177.22	−464.838	−161.221
coulomb part	Coulomb (SR)	−124335	−103970	−19286.8
	Coul. recip.	4192.18	1173.28	3359.21
Summation		−138180.24	−110982.618	−19221.791

Table R6. The related energies in calculating the interaction energy between PTFMA and FEP molecule, ΔE(PTFMA-FEP) = −29380.902 (kJ/mol)

Energy (kJ/mol)		*E*(PTFMA+FEP)	*E*(PTFMA)	*E*(FEP)
vdw part	LJ(SR)	−91304.88	−7721.06	−59369.7
	Disper. corr.	−6910.74	−464.838	−3784.96
coulomb part	Coulomb (SR)	44733.54	−103970	150710
	Coul. recip.	5347.44	1173.28	4673.54
Summation		−48134.64	−110982.618	92228.88

5. On page 7, line 7-13, Figures 2d & 2e: In Figure 2, the authors presented the coordination number of Li+ with TFSI, FEC, FEP, and PTFMA in WSPE. However, the solvation structure and coordination number (CN) of Li^+ in liquid electrolytes were not discussed. Specifically, does the interaction between Li^+ cation and FEP in liquid electrolytes become stronger, potentially increasing the CN of Li^+ with FEP? Or does TFSI- maintain a higher CN due to its role as the counterion for Li^+? Again, the authors should compare the simulation results of the solvation structure with and without FEC to confirm that WSPE functions as a weakly-solvated topological polymer electrolyte. This comparison would provide a clearer understanding of how the solvation structures differ between WSPE and liquid electrolytes.

Response: Thank you very much for your valuable comments.

We fully agree with you that the additional comparison would further clarify the interaction between FEP and PTFMA on the solvation structure. We added the

corresponding discussion in two aspects: (1) the solvation structure of the liquid electrolyte and (2) the solvation structure of the FEC-free polymer electrolyte (FEC-free PE).

(1) The solvation structure of the liquid electrolyte

The radial distribution function (RDF) and the corresponding coordination number (CN) in the liquid electrolyte are shown in Fig. R8. In the RDF, the initial peak corresponding to Li^+–O (FEP) appears at 2.04 Å, which is significantly shorter than that of Li^+–O ($TFSI^-$) (2.12 Å) and Li^+–O (FEC) (2.15 Å). Compared with WSPE, Li^+ is obviously more tightly bound to FEP, while the binding to $TFSI^-$ is significantly weaker (the initial peaks corresponding to Li^+–O (FEP) and Li^+–O ($TFSI^-$) in WSPE appear at 2.12 Å and 2.06 Å, respectively) (Fig. R9). At a distance of 3.0 Å from Li^+, the CNs of FEP, FEC and $TFSI^-$ are 2.85, 0.59 and 1.96, respectively. It can be seen that in the liquid electrolyte, the first Li^+ solvation sheath contains more FEP, forming a strong solvation structure dominated by solvent molecules. The ratio of CNs of $TFSI^-$ to solvent molecules in the liquid electrolyte is 0.57, much lower than that of 2.3 in WSPE. This suggests that the introduction of the PTFMA significantly alters the coordination environment of Li^+ and promotes the formation of an anion-dominated weak solvation structure.

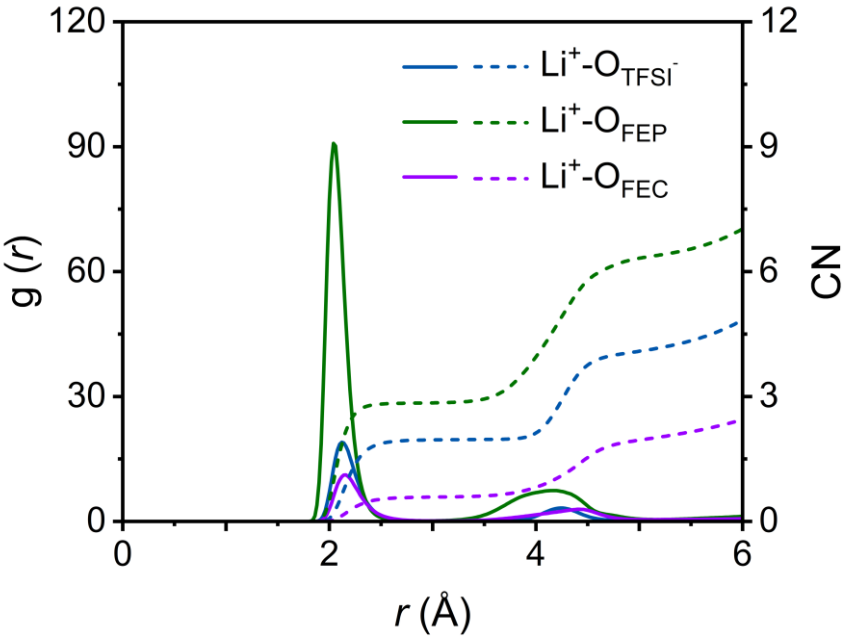

Fig. R8 (Supplementary Fig. 5 in revised Supplementary information). RDFs and CNs of Li^+ in the liquid electrolyte.

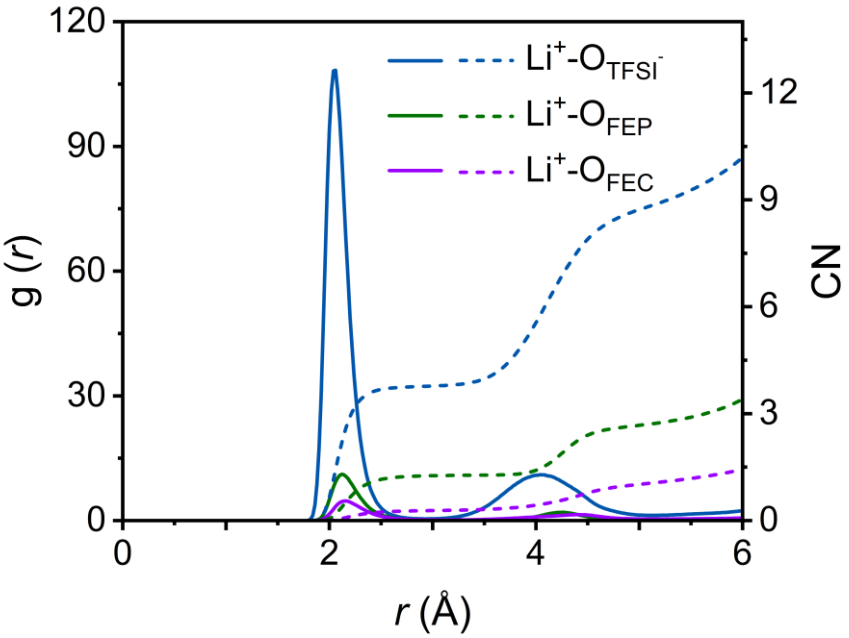

Fig. R9. RDFs and CNs of Li^+ in the WSPE.

To sum up, the interaction between Li^+ and FEP in the liquid electrolyte is stronger than that in WSPE, resulting in a higher CN of Li^+ and FEP in liquid electrolyte. The above simulation results have been added in the revised Supplementary information as Supplementary Fig. 5 and the discussion has been added in revised manuscript (Paragraph 2, Page 7).

(2) The solvation structure of the FEC-free PE

The RDF and the corresponding CN in the FEC-free PE are shown in Fig. R10. In the RDF, the initial peaks corresponding to Li^+–O ($TFSI^-$) and Li^+–O (FEP) appear at 2.04 Å and 2.12 Å, respectively, which are in general agreement with the simulation results of WSPE. At a distance of 3.0 Å, the CNs of FEP and $TFSI^-$ are 1.54 and 3.74, respectively (the CN ratio of $TFSI^-$ to solvent molecule is 2.4, which are also highly consistent with that in WSPE). This suggests that FEC has no significant effect on the solvation structure of the WSPE, i.e., the formation of the weak solvation structure is attributed to the interactions between the FEP and PTFMA.

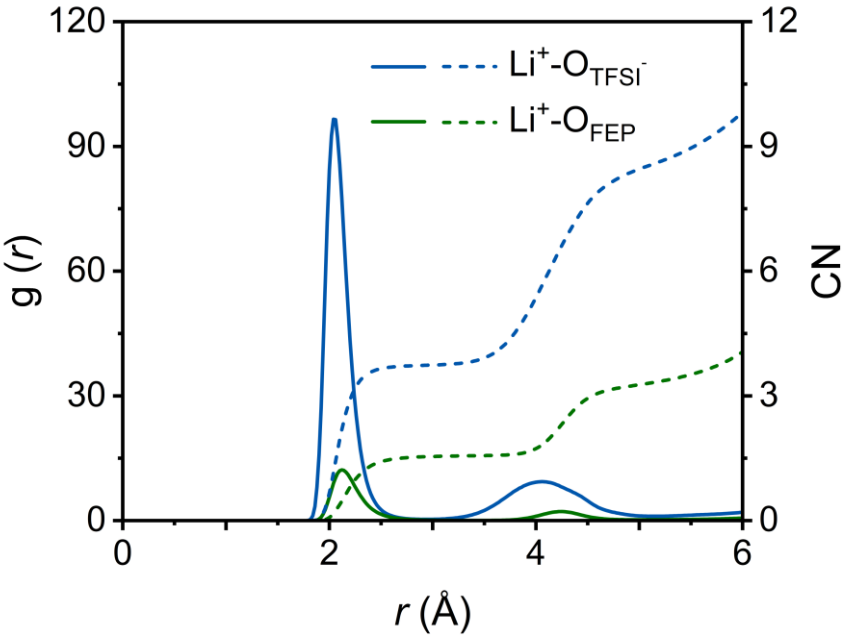

Fig. R10. RDFs and CNs of Li^+ in the FEC-free PE.

The above simulation results demonstrate that the interaction of FEP with the PTFMA significantly increases the coordination of Li^+ with $TFSI^-$, weakens the coordination of Li^+ with solvent molecules, and effectively induces the formation of the weak solvation structure.

6. On page 7, line 18-20, Figure 2f: The authors mentioned that "The presence of a large number of CIPs minimizes solvent polarization and keeps the FEP away from the electrode to prevent side reactions."; However, this sentence is not clear to this reviewer. Could the authors further explain why a higher CIP number would cause FEP to stay away from the electrode?

Response: Thank you for your comments.

Firstly, in the liquid electrolyte, Li^+ is significantly solvated, resulting in weak Li^+–$TFSI^-$ interactions and much free $TFSI^-$. During the charging process, the cluster formed by Li^+ and solvent molecules moves toward the Li anode, and FEP preferentially contacts the anode surface due to its strong coordination with Li^+ and is reduced to form unstable SEI. At the same time, on the cathode side, a large number of free $TFSI^-$, which lacks Li^+ binding, would accumulate on the surface of the cathode. The newly stripped Li^+ from the cathode will be captured by the aggregated anions,

further aggravate the polarization. The free solvent molecules on the surface of the cathode which cannot be coordinated with Li^+ are also prone to be oxidized under high voltage and decompose to form unstable CEI.

For WSPE, a large number of CIPs are formed, effectively reducing the free $TFSI^-$ content. During the charging process, the Li^+ solvation clusters dominated by $TFSI^-$ move toward the Li anode. Due to the strong Li^+–$TFSI^-$ interaction, $TFSI^-$ can preferentially contact with the Li anode surface and be reduced to form a LiF-rich SEI layer. In contrast, FEP solvent molecules are excluded to the periphery of the Li^+ solvation sheath, relatively far away from the Li anode, and decomposition is significantly suppressed. In addition, free $TFSI^-$ can't be accumulated on the surface of the cathode due to the stronger Li^+–$TFSI^-$ coordination. The newly stripped Li^+ from the cathode can coordinate with the free solvent molecules and move rapidly to the anode, which helps to stabilize the solvent and inhibits the oxidative decomposition of solvent on the cathode surface.

In the study of the fundamental relationship between Li^+ solvation structure and electrochemical performance, Zou et al. propose a novel interfacial model that elaborates on the above process in more detail, and experimentally demonstrates that the electrolyte system containing a large amount of CIP exhibits high electrolyte and electrode stability.[1] In summary, a large number of CIPs can reduce the solvation polarization while keeping the solvent away from the electrodes, thus inhibiting the decomposition of the solvent.

7. On page 7, line 27-30, Figures 2g and 2h: The authors discussed the diffusion coefficients of Li^+, $TFSI^-$, and FEP, obtained from the MD simulation, noting that FEP exhibits a higher diffusion coefficient than the two ions. This raises the question of why FEP, interacting with PTFMA through double dipole coupling, has a higher diffusion coefficient. Does this imply that FEP can fast move to the electrode? If so, this interpretation seems inconsistent with the FTIR results. Furthermore, the diffusion coefficient of Li^+ is similar to one of $TFSI^-$. This may be another case that is contradictory to the high lithium transference number (0.83). Could the authors clarify how similar diffusion coefficients between Li^+ and $TFSI^-$ contribute to a high lithium transference number?

Response: Thank you very much for your valuable comments.

(1) Generally, in the absence of an applied electric field, the diffusion coefficient of neutral organic molecules, e.g. FEP is much higher than those of charged ions, e.g. Li^+ and $TFSI^-$. Because there is a stronger interaction between the Li^+ and $TFSI^-$, which would limit the diffusion of the ions. For WSPE, the double dipole coupling of FEP and PTFMA would affect the diffusion of FEP. We fitted the mean-square displacement (MSD) curves of each species in the liquid electrolyte with time (Fig. R11a), and the diffusion coefficients were calculated as shown in Fig. R11b. The results indicate that the diffusion coefficient of FEP decreased from 3.33×10^{-10} m^2 s^{-1} in liquid electrolyte to 1.93×10^{-10} m^2 s^{-1} in WSPE. This suggests that the double dipole coupling interaction between FEP and PTFMA indeed effectively confines the diffusion of FEP.

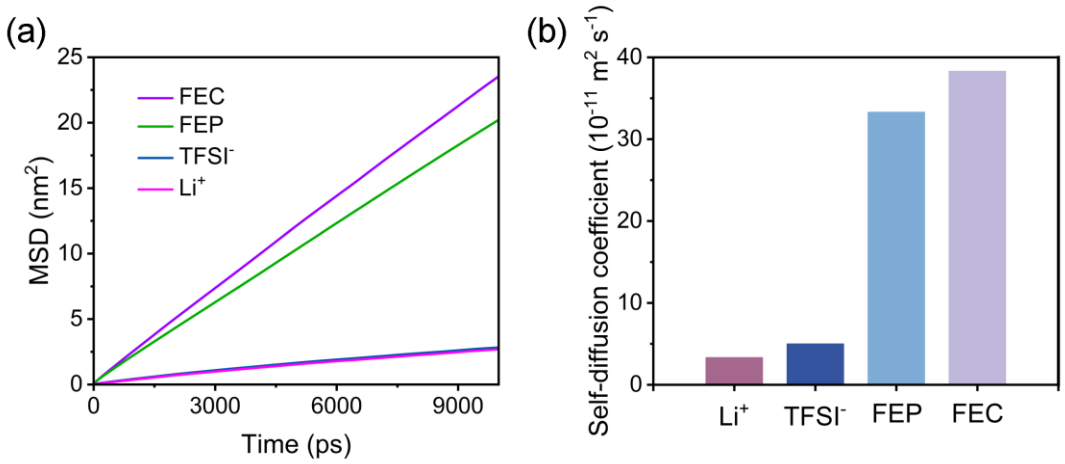

Fig. R11. (a) MSD-time curves and (b) the corresponding diffusion coefficients of liquid electrolyte components.

Although FEP has a high diffusion coefficient, the strong interaction between FEP and PTFMA framework can significantly change the electron cloud distribution of the FEP, weakening the negative electronegativity of the O atoms on the FEP, and thus weakening the coordination of the FEP to Li^+. Therefore, a weak solvation structure dominated by anions is still observed in WSPE, which does not contradict the FTIR results.

(2) Simulation conditions are an important factor in the deviation of simulation results from experimental values. To the best of our knowledge, no optimized simulation model has been reported for the crosslinked system. Due to the difficulty of calculating a crosslinked system, we have followed the work of Zhou et al. to simplify the crosslinking framework with 10 repeated TFMA units.[2] That is, PTFMA chains have

some mobility in MD simulations. As a result, the binding effect of the framework towards $TFSI^-$ is weakened accordingly, which leads to high diffusion coefficients of $TFSI^-$ in the simulation results and consequently to lower Li^+ transference number. In fact, Zhou et al. obtained a diffusion coefficient of Li^+ smaller than that of anions by MD simulations, and experimentally measured an Li^+ transference number of 0.61. The limitations of the MD simulation condition for the crosslinked system would lead to unavoidable deviations of it from the experimental values,[2–4] whereas the comparison between samples from simulation results by using the same conditions can be used to analyze our experimental results.

8. On page 8, Figure 3f: The authors present the cell performances at RT, LT, and HT. However, the LT cycling performance was conducted only at a low C-rate (0.2 C). Is there a specific reason for this?

Response: Thank you very much for your valuable comments. According to your comments, we performed the LT cycling test at a high C-rate (0.5 C). The cycling performance of the Li/WSPE/NCM811 cell at 0.5 C and –20 °C is shown in Fig. R14. After 200 cycles, the Li/WSPE/NCM811 cell still delivers a discharge specific capacity of 109.1 mAh g^{-1}, which is 95.5% of the initial capacity. We have added Fig. R12 in the revised Supplementary information as Supplementary Fig. 26 and added the corresponding description in the revised manuscript (Paragraph 1, Page 11).

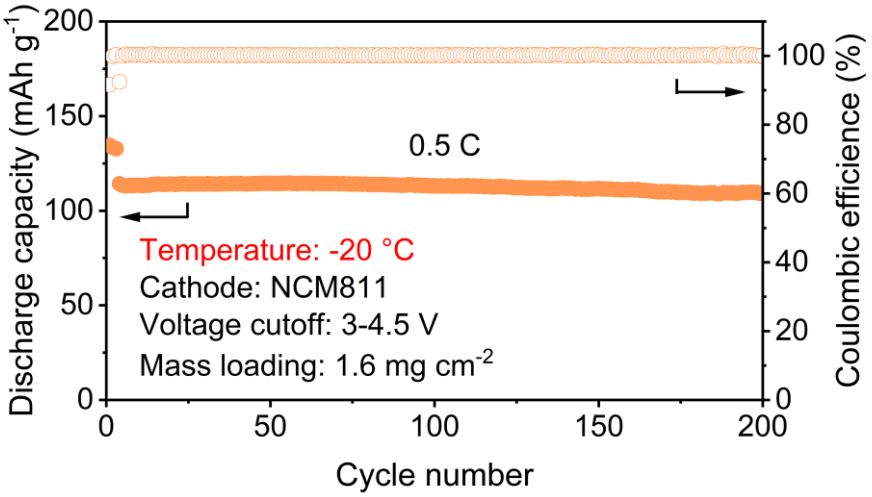

Fig. R12 (Supplementary Fig. 26 in revised Supplementary information). Cycling performance of the Li/WSPE/NCM811 cell at −20 °C and 0.5 C.

9. On page 9, line 11-16, Figures S13 and S14: Figures S13 and S14 show the EIS results of liquid electrolyte (LE) and WSPE at different temperatures. It would be helpful to include the equivalent circuit and a table of R_{ct} and R_{SEI} values in SI. To demonstrate that the lower resistance of WSPE after cycling, compared to the liquid electrolyte, is due to the stable EEI generation, it would be beneficial for the authors to provide the interfacial resistance of both WSPE and LE before cycling.

Response: Thank you very much for your suggestions.

We have added the corresponding equivalent circuit (Fig. R13, Supplementary Fig. 23 in the revised Supplementary information) and the table of R_{ct} and R_{SEI} values (Table R7, Supplementary Table 2 in the revised Supplementary information) in the revised SI.

The variation of interfacial impedance along with cycling in Fig. R7 for Li/NCM811 cells using different electrolytes is shown in Fig. R14. Before cycling, the EIS plot of the Li/NCM811 cell contains only one semicircle, representing the charge transfer resistance (R_{ct}). After 10 cycles of activation, a new semicircle in the middle-frequency region indicates the generation of an interfacial layer.[5] As shown in Fig. R14a, the interfacial impedance of the Li/WSPE/NCM811 cell is increased and then decreased rapidly and stabilized afterwards, which indicates that the interfacial layer generated by WSPE has a high ionic conductivity and densifies rapidly with cycling. In contrast, the interfacial impedance of liquid batteries is increased continuously with cycling (Fig. R14b), which is caused by the constant fragmentation of the unstable interfacial layer and the unceasing decomposition of the electrolyte, leading to the decay of the capacity. Similar to liquid batteries, the interfacial impedance of FEP-free PE and PTFMA-free PE batteries rises continuously (Figs. R14c, d). This suggests that all the control samples (liquid electrolytes, FEP-free PE and PTFMA-free PE) don't have the ability to generate stable interfacial layers. Instead, WSPE can form a stable interfacial layer during cycling, thus bringing in outstanding cycling performance to high-voltage lithium metal batteries. We have added Fig. R14 in the revised Supplementary information as Supplementary Fig. 20 and added the corresponding description in the revised manuscript (Paragraph 1, Page 10).

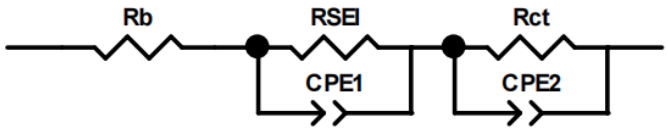

Fig. R13 (Supplementary Fig. 23 in revised Supplementary information). The equivalent circuit diagram of EIS for Li/NCM811 cells.

Table R7 (Supplementary Table 2 in revised Supplementary information). The impedance values of the WSPE cell and the liquid cell at different temperatures.

	WSPE			**Liquid electrolyte**		
	$R_b(\Omega)$	$R_{SEI}(\Omega)$	$R_{ct}(\Omega)$	$R_b(\Omega)$	$R_{SEI}(\Omega)$	$R_{ct}(\Omega)$
80 ℃	2.2	22.7	12.7	2.7	60.2	32.2
40 ℃	2.8	29.2	26.5	3.2	75.8	50.8
0 ℃	4.5	123.4	295.8	5.7	651.4	814.5
-10 ℃	5.3	303.0	1037	6.1	1802	2082
-20 ℃	7.7	814.1	1728	8.5	5544	6132

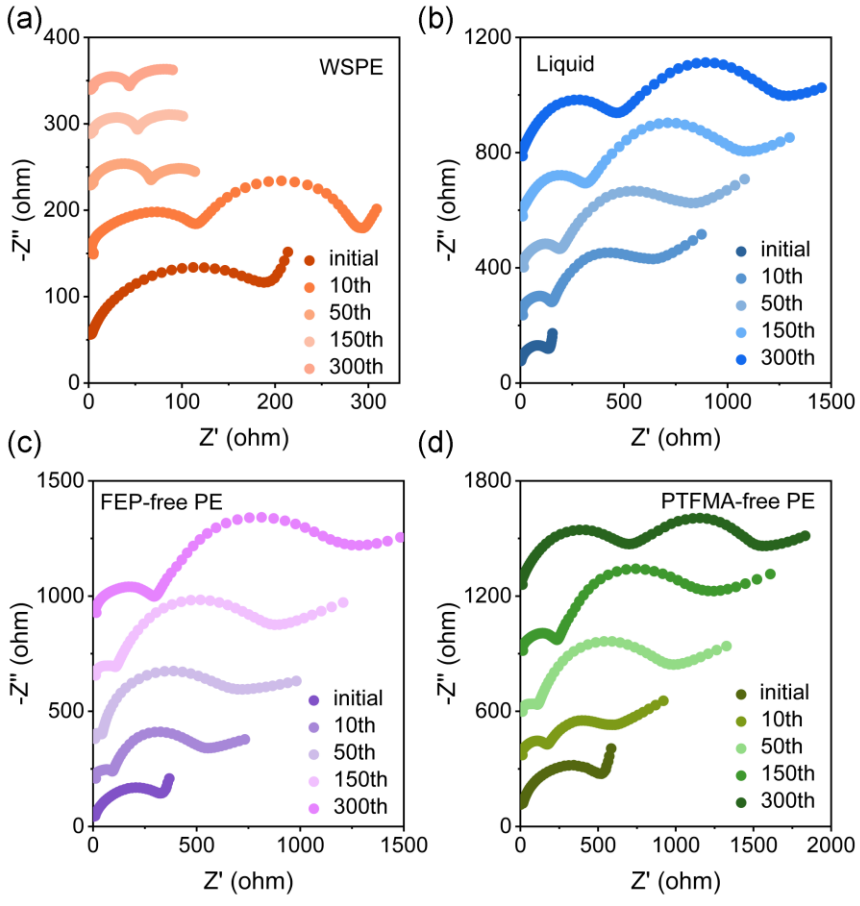

Fig. R14 (Supplementary Fig. 20 in revised Supplementary information). EIS plots of Li/NCM811 cells using (a) WSPE, (b) liquid electrolyte, (c) FEP-free PE and (d) PTFMA-free PE during cycling.

10. On page 10, Line 8: The authors successfully implemented a pouch cell using a high mass loading (23.4 mg/cm^2) cathode and a thin Li foil anode with a thickness of 50 μm. Given that the N/P ratio of the pouch cell is expected to be low, it is recommended that the authors provide the N/P ratio value in the manuscript for clarity.

Response: Thank you very much for your valuable suggestion.

According to your comments, we calculated the N/P ratio of the pouch cell as 2.9 and provided it in the revised manuscript (Paragraph 3, Page 11).

11. On page 10, Line 22, Figure 5a: The authors mentioned that the cell is stable when applied with various current densities up to 1 mA/cm^2. However, in Figure 5a, the specific current densities applied to the cell are not clearly indicated. Please provide detailed information on the range of current densities that was applied to the cell in the figure.

Response: Thank you very much for your suggestion. We cycled at each current density 10 times in increments of 0.1 mA cm^{-2} over the range of 0.1 to 1 mA cm^{-2} and finally returned the current density to 0.1 mA cm^{-2}. According to your suggestion, we have added the corresponding current density information in Fig. 5a in the revised manuscript.

Response to Reviewer #2:

1. This paper does not make sense to me, and I suggest its rejection. This would be a unique set-up, having so very low dependence on temperature. This is not consistent with any other observations on solid polymer electrolytes, and barely with liquid electrolytes. The authors have no reasonable explanation for this observation, if it in fact exists. Then, it is not a polymer electrolyte — it is basically a liquid FEC/FEP

electrolyte (heavily fluorinated), contained in a polymer matrix. It is clearly a gel, but the entire discussion is written in the context of it being solid polymer electrolyte. If compared with heavily fluorinated liquid electrolytes, the results are not really that impressive. The gel electrolyte contains many components, but is poorly described in terms of composition and preparation.

Then, the entire analogy with a biological system is misleading. I would assume it is an analogy also, rather than an inspiration. This analogy is however just confusing for the reader, and likely incorrect if the true modes of structural organization and ionic transport would be determined.

Response: Thank you very much and we very appreciate your comments on our manuscript.

We have carefully considered your comments and made major modification on the manuscript. For your concerns, our response can be summarized as follows: (1) the explanation for the low dependence on temperature; (2) the definition of our electrolyte; (3) the description of the composition and the preparation; and (4) the interpretation on the bioinspiration.

(1) The explanation for the low dependence on temperature

The low dependence on temperature of our electrolyte is attributed to the unique ion transport mechanism, the construction of the Li^+ weak solvation structure, and the formation of the high ionic conductivity interfacial layers. The detailed explanation can be described as below:

a. The unique ion transport mechanism

In conventional polymer electrolytes such as PEO, Li^+ transport depends on the movements of the chain segments, and Li^+ can transport by constant coupling/decoupling with the O atoms of the PEO. Therefore, the PEO-based polymer electrolytes can only be applied at high temperatures and the chain segments are frozen at low temperatures.[6,7] Thus, PEO-based electrolytes exhibit a significant temperature dependence.

In liquid electrolytes, Li^+ forms solvation clusters with solvent molecules and anions and relies on the rapid diffusion of solvent for rapid transport in the form of clusters. The Li^+ transport rate at this time is closely related to the cluster size. As the temperature decreases, the thermal motion of the particles slows down and the interactions between the particles are relatively enhanced, and the Li^+ cluster size

increases accordingly, leading to an increase in the hydrodynamic radius and hindering the transport, which is the main reason for the significant decrease of the ionic conductivity at low temperatures.[8]

Although Li^+ in WSPE is also transported in the form of solvation clusters, such clusters are neither fully decoupled from the chain segments of PTFMA, nor increased with temperature due to polymer framework restriction. A large number of FEP solvent molecules exist at the periphery of the Li^+ solvation clusters, and there is a dynamic interaction between the FEP and PTFMA frameworks. Thus, the Li^+ solvation clusters can achieve rapid diffusion along the framework by the periphery FEP constant coupling/decoupling with the PTFMA side chains. As the temperature decreases, the strong double dipole coupling interactions between the framework and the FEP molecules limit the enhancement of the interactions between Li^+ and the solvent molecules. To clarify, the solvation structure of WSPE at different temperatures has been analyzed by MD simulation. Shown in Fig. R1, the position of the Li^+ solvation sheath changes very little with the temperature decreases. This result implies that the size of the Li^+ solvation clusters does not change much with temperature. Therefore, the ionic conductivity of WSPE exhibits a low dependence on temperature.

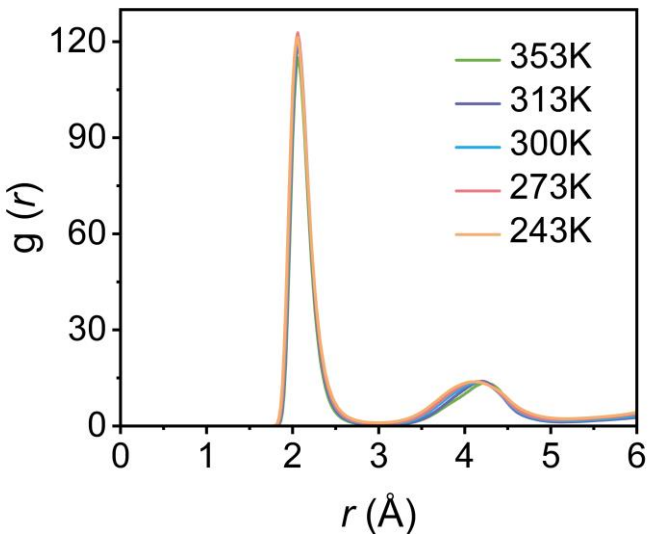

Fig. R1. The RDF of Li^+ in WSPE under different temperatures.

b. The Li^+ weak solvation structure

Unlike the approach of constructing anions-dominated solvation structures by increasing the lithium salt concentration in high concentration or localized high concentration electrolytes, we achieve the weak solvation structure through the

competitive coordination of the framework with Li^+ to the FEP. It is known that high lithium salt concentration would bring in significant increase in electrolyte viscosity and cluster size at low temperatures. Through double dipole coupling interactions, we only need a lithium salt concentration of 1 M to achieve a weak solvation structure. This is an important reason for maintaining the high ionic conductivity of WSPE at low temperatures.

Moreover, sluggish interfacial ion transport is often a limiting factor for low-temperature performance, and the weak solvation structure can significantly reduce the Li^+ desolvation energy. Shown in Fig. R2, the downfield shift of the ^7Li NMR peak in WSPE supports the formation of a weakened coordination environment of Li^+.[9] This facilitates the desolvation of Li^+ at the interface. The coordination numbers (CN) of the components around Li^+ vary with temperature as shown in Figs. R3a-c. As the temperature decreases, the CN of $TFSI^-$ around Li^+ decreases and the CN of FEP and FEC solvent molecules increases. Nonetheless, even at the low temperature of –30 °C, the CN of $TFSI^-$ is still higher than that of the FEP at a distance of 3 Å from Li^+. It suggests that the Li^+ solvation structure in WSPE at low temperatures is still a weak solvation structure dominated by anions.

These results have been added in the revised Supplementary information as Supplementary Fig. 6 and corresponding discussion has been added in the revised manuscript (Paragraph 1, Page 8).

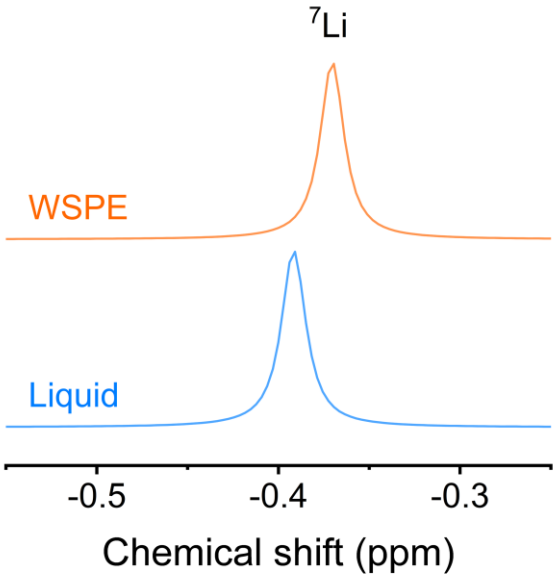

Fig. R2 (Supplementary Fig. 6 in revised Supplementary information). ^7Li NMR of liquid electrolyte and WSPE.

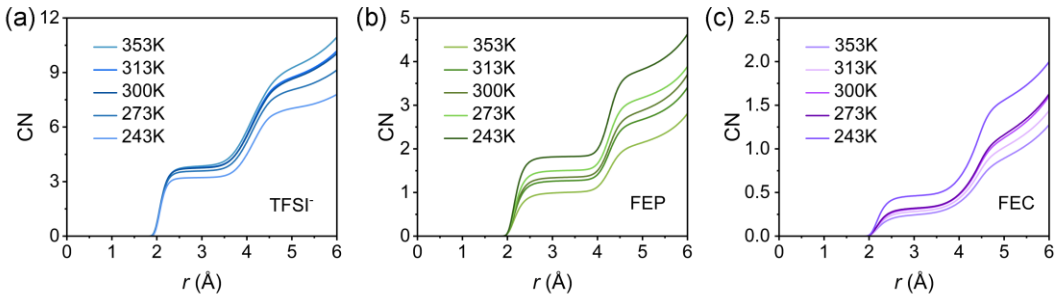

Fig. R3. CNs of Li^+ with (a) $TFSI^-$, (b) FEP and (c) FEC in WSPE at different temperatures.

c. The formation of the high ionic conductivity interfacial layer

The impedance of Li^+ across the SEI layer is an important factor limiting the low-temperature performance. The anion-dominated solvation structure forms a high ionic conductivity interfacial layer enriched with inorganic LiF, Li_3N and Li_2O (Figs. 5c-h), which would be another factor contributing to the low dependence on temperature of WSPE.[10]

In summary, the unique double dipole coupling interactions between the framework and FEP solvent in WSPE induce a unique ion transport mechanism, a Li^+ weak solvation structure, and an inorganic-rich interfacial layer with high ionic conductivity. These bring in a temperature-independent microscopic solvation structure and mesoscopic cluster structure in WSPE, resulting in low dependence on temperature.

(2) The definition of electrolyte in this work

The solid matrix in conventional gel electrolytes only serves to physically encapsulate the liquid electrolyte to prevent liquid leakage. The electrochemical performance of the gel electrolyte depends on the composition of the liquid in it. However, in our electrolyte, the designed strong interaction between the solvent and the polymer matrix plays a key point in the electrolyte state, solvation structure, and electrochemical performance. The electrolyte in this work is a unique polymer electrolyte that is very different with conventional gels.

To clarify the difference between WSPE and conventional gel electrolytes, we prepared two sets of conventional gel electrolytes as comparison samples. One group replaces FEP in WSPE with an equivalent amount of FEC (FEP-free PE), and another group replaces the PTFMA framework in WSPE with an equivalent amount of PEGDA (PTFMA-free PE). The associated results are as follows:

a. Solid-like states induced by unique double dipole coupling interactions

As shown in Fig. R4, an additional experiment has been carried out to further demonstrate that the double dipole coupling interaction is unique to the FEP and PTFMA. The TFMA was polymerized firstly to obtain the linear PTFMA, and then equal amounts of FEP and FEC solvents were added, respectively (notes as PTFMA+FEP and PTFMA+FEC). For PTFMA+FEP, after keeping at room temperature for 8 h, a transparent homogeneous bulk having solid-like state is presented without fluidity. As a contrast, there is still a clear solid-liquid interface between FEC and PTFMA for PTFMA+FEC. These results suggest that there is a strong interaction between PTFMA and FEP, leading to a solid-like state at room temperature. These results have been added in the revised Supplementary information as Supplementary Fig. 4 and corresponding discussion has been added in the revised manuscript (Paragraph 1, Page 7).

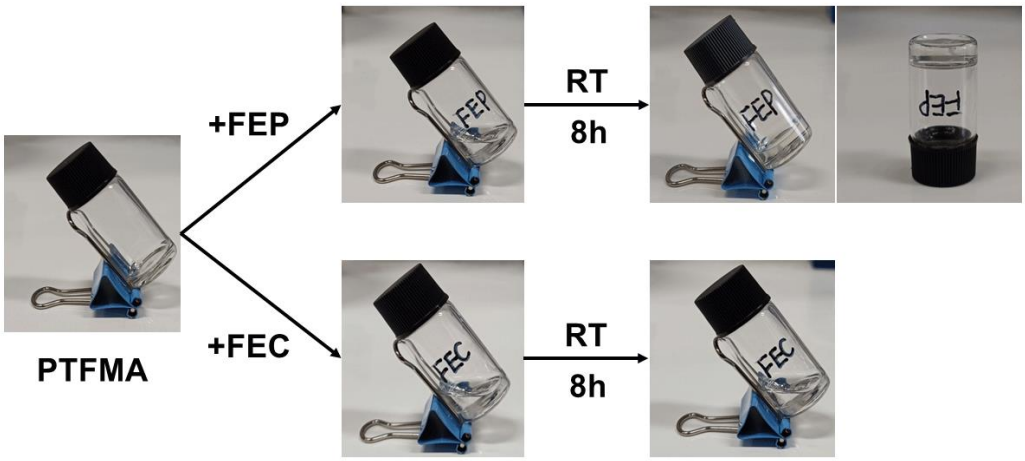

Fig. R4 (Supplementary Fig. 4 in revised Supplementary information). The diagram of static experiment at room temperature.

To further demonstrate the unique binding effect of the FEP with PTFMA framework, the differential scanning calorimetry (DSC) measurements of PTFMA-free PE and WSPE have been conducted as shown in Fig. R5. When the liquid electrolyte was encapsulated with pure PEGDA matrix, the vaporization temperature of FEP was 90.1 °C. In contrast, the vaporization temperature of FEP in WSPE was significantly increased to 104.4 °C, and the endothermic reaction enthalpy of vaporization was also

significantly increased from 16.8 J g^{-1} in PTFMA-free PE to 70.2 J g^{-1} in WSPE. It is confirmed that the PTFMA matrix has a strong binding effect on FEP and can effectively inhibit the volatilization of FEP solvents.

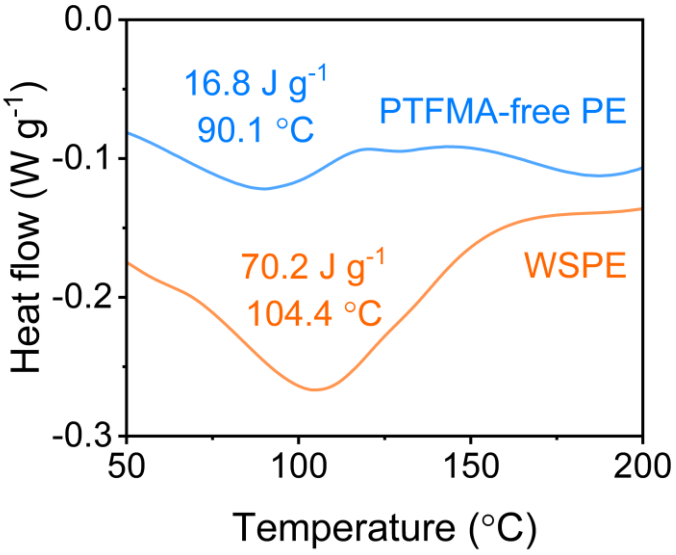

Fig. R5. The DSC curves of PTFMA-free PE and WSPE.

This strong interaction between FEP with PTFMA makes our electrolyte exhibit a solid-like state at room temperature, which is clearly different from the gel system in the conventional sense.

b. Weak solvation structure induced by double dipole coupling interactions

The FTIR of a conventional gel electrolyte (FEP-free PE) is shown in Fig. R6a. The precursor of FEP-free PE showed a distinct peak of C=C bond at 1640 cm^{-1}. After curing at 70 °C for 5 h, the C=C peak disappeared obviously, indicating the completely polymerization of TFMA. The S−N−S stretching vibrational peaks of $TFSI^-$ are shown in Fig. R6b. $TFSI^-$ in the FEC liquid electrolyte (1M LiTFSI in FEC) exists mainly in the form of free anions (FAs), and the addition of PTFMA framework has no significant effect on the solvation structure. FEP-free PE is still dominated by FAs, suggesting that the polymer matrix in conventional gel systems does not affect the solvation structure of the electrolyte. Further, a comparison of the solvation structures of the liquid electrolyte (1M LiTFSI in FEP with 5 wt% FEC), PTFMA-free PE and WSPE is shown in Fig. R7. There is no obvious difference between the liquid electrolyte and PTFMA-free PE, which are both dominated by FAs without ion aggregates (AGGs). In contrast, the peak position of WSPE shows a significant blue shift, indicating that the

introduction of the PTFMA framework changes the solvation structure of the liquid electrolyte from FAs-dominated to contact ion pairs (CIPs)-dominated.

Based on the analysis, it is reasonable to conclude that the weak solvation structure forms only when FEP and PTFMA coexist. The solvation structure of conventional gel electrolytes is determined by their liquid components, and the polymer matrix does not affect their solvation structures obviously. These results have been added in the revised Supplementary information as Supplementary Figs. 7 and 8.

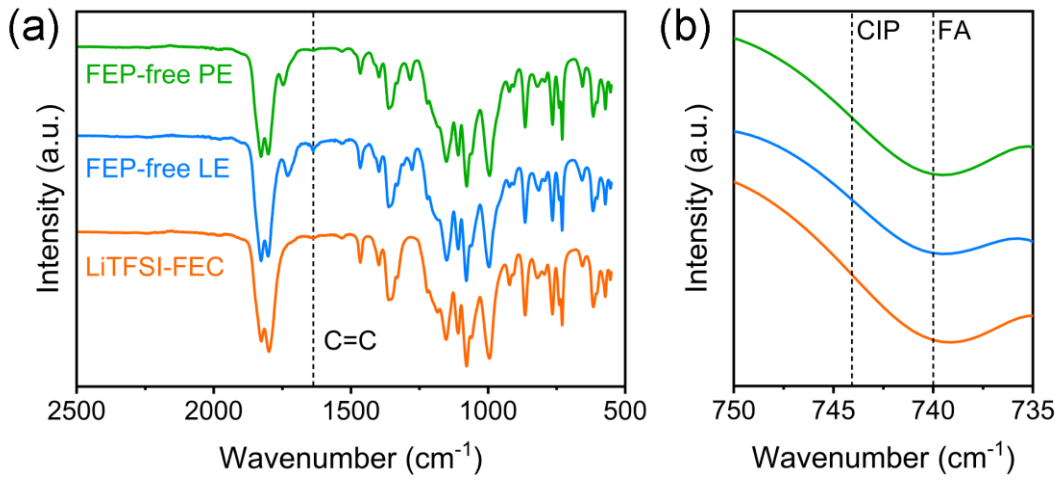

Fig. R6 (Supplementary Fig. 7 in revised Supplementary information). (a) FTIR spectra and (b) S−N−S stretching of $TFSI^-$ of FEC liquid electrolyte, FEP-free LE and FEP-free PE.

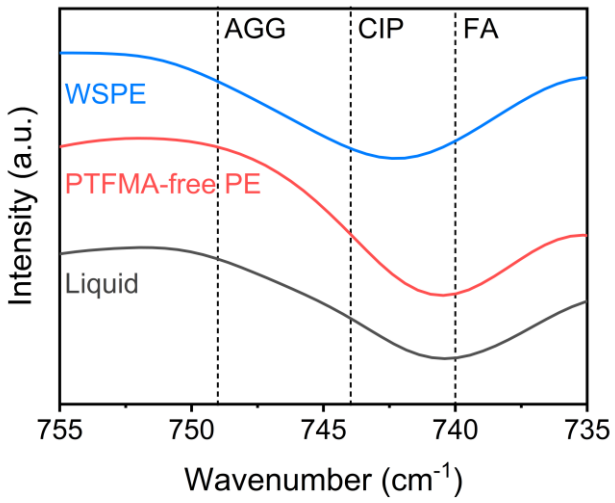

Fig. R7 (Supplementary Fig. 8 in revised Supplementary information). FTIR spectra of liquid electrolyte, PTFMA-free PE and WSPE.

c. Improved electrochemical performance due to the double dipole coupling interactions

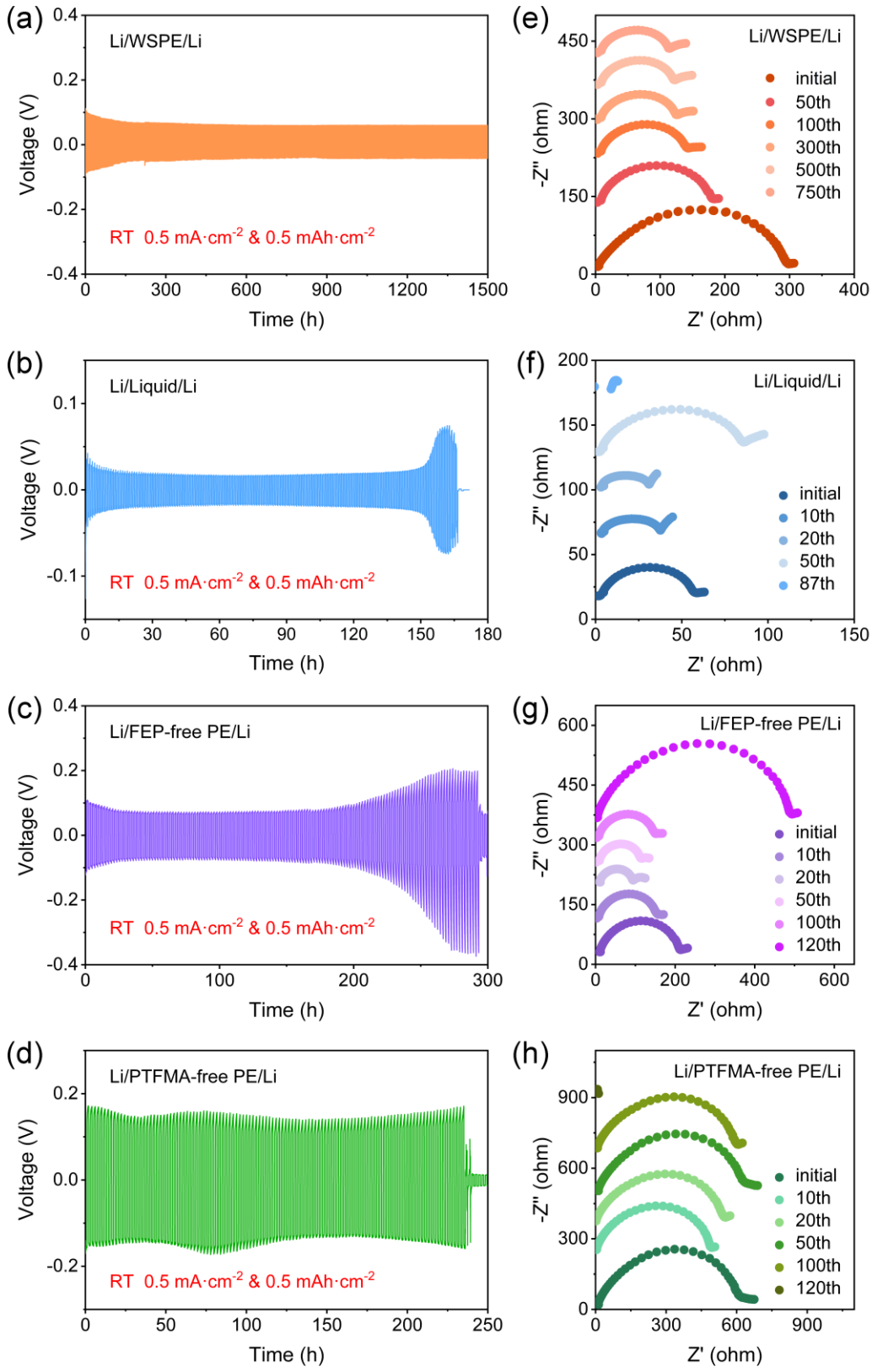

Fig. R8 (Supplementary Figs. 30 and 31 in revised Supplementary information).

Galvanostatic cycling performance of Li symmetric cells using (a) WSPE, (b) liquid electrolyte, (c) FEP-free PE and (d) PTFMA-free PE. EIS plots during cycling of Li symmetric cells using (e) WSPE, (f) liquid electrolyte, (g) FEP-free PE and (h) PTFMA-free PE.

Attributed to the weak solvation structure and unique ion transport mechanism, WSPE exhibits excellent electrochemical performance. The cycling performance of the Li symmetric cells assembled with WSPE, liquid electrolyte, FEP-free PE and PTFMA-free PE at 0.5 mA cm^{-2} and 0.5 mAh cm^{-2} is shown in Fig. R8. As for the Li/WSPE/Li cell, it can be stably cycled at room temperature for more than 1500 h without short-circuiting (Fig. R8a). The interfacial impedance of the cell decreases and stabilizes with cycling (Fig. R8e). After 100 cycles, the interfacial impedance of the cell stabilized at about 120 Ω, indicating the formation of a stable high conductivity SEI layer. In contrast, liquid electrolyte, FEP-free PE and PTFMA-free PE cells were short-circuited at 166 h, 293 h and 236 h, respectively (Figs. R8b-d). During cycling, the interfacial impedance of the three control samples showed a tendency to decrease firstly and then increase before short circuit. (Figs. R8f-h). That means the generated SEI layer is unstable and cannot effectively inhibit the decomposition of the electrolyte on the Li surface in the three control samples. These results have been added in the revised Supplementary information as Supplementary Figs. 30 and 31 and corresponding discussion has been added in the revised manuscript (Paragraph 3, Page 12).

The exchange current density (I_0) extracted from Tafel plots was used to quantitatively study interfacial Li^+ transfer kinetics at −20 °C (Fig. R9). The I_0 in WSPE (0.38 mA cm^{-2}) is markedly larger than those in liquid electrolyte (0.29 mA cm^{-2}), PTFMA-free PE (0.21 mA cm^{-2}) and FEP-free PE (0.16 mA cm^{-2}), implying fast interfacial Li^+ transfer kinetics and the construction of highly conductive SEIs in WSPE at low temperature.[11] These results have been added in the revised Supplementary information as Supplementary Fig. 24 and corresponding discussion has been added in the revised manuscript (Paragraph 2, Page 10).

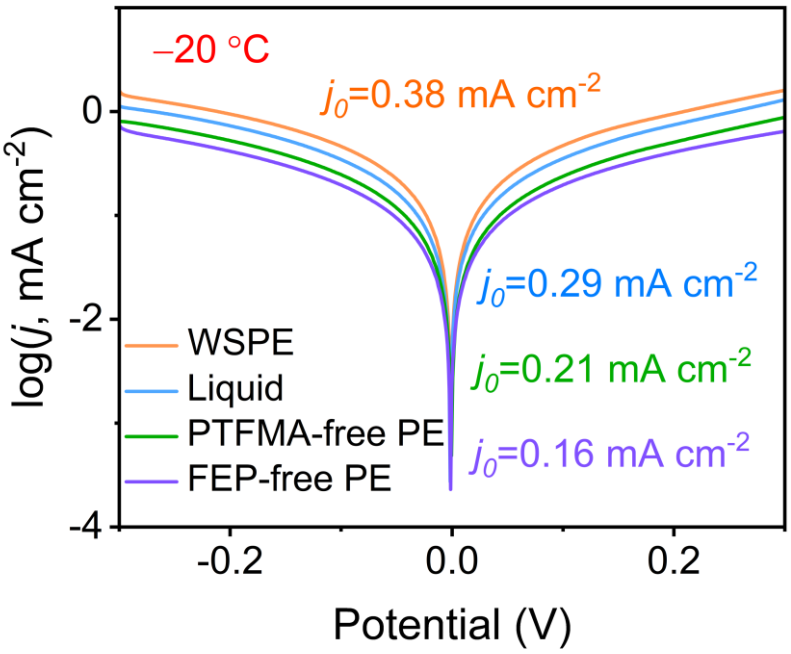

Fig. R9 (Supplementary Fig. 24 in revised Supplementary information). Tafel plots of Li plating/stripping in different electrolytes at −20 °C.

The cycling performance of Li/NCM811 cells assembled with WSPE, liquid electrolyte, FEP-free PE and PTFMA-free PE at 1 C is shown in Fig. R10. The Li/WSPE/NCM811 cell shows the most excellent cycling stability, delivering a capacity of 120.8 mAh g^{-1} after 300 cycles, with an average capacity decay of only 0.087% per cycle. As for the control, cells based on liquid electrolyte and FEP-free PE, high initial capacity of 167.8 mAh g^{-1} and 169.3 mAh g^{-1} are measured, respectively. However, only 51.4% and 50.5% of the initial capacities retain after 300 cycles, corresponding to liquid electrolyte and FEP-free PE cells, respectively. Similarly, the Li/PTFMA-free PE/NCM811 cell delivers a capacity of 63.2 mAh g^{-1} after 300 cycles, which is 43.3% of the initial capacity. These results have been added in the revised Supplementary information as Supplementary Fig. 13.

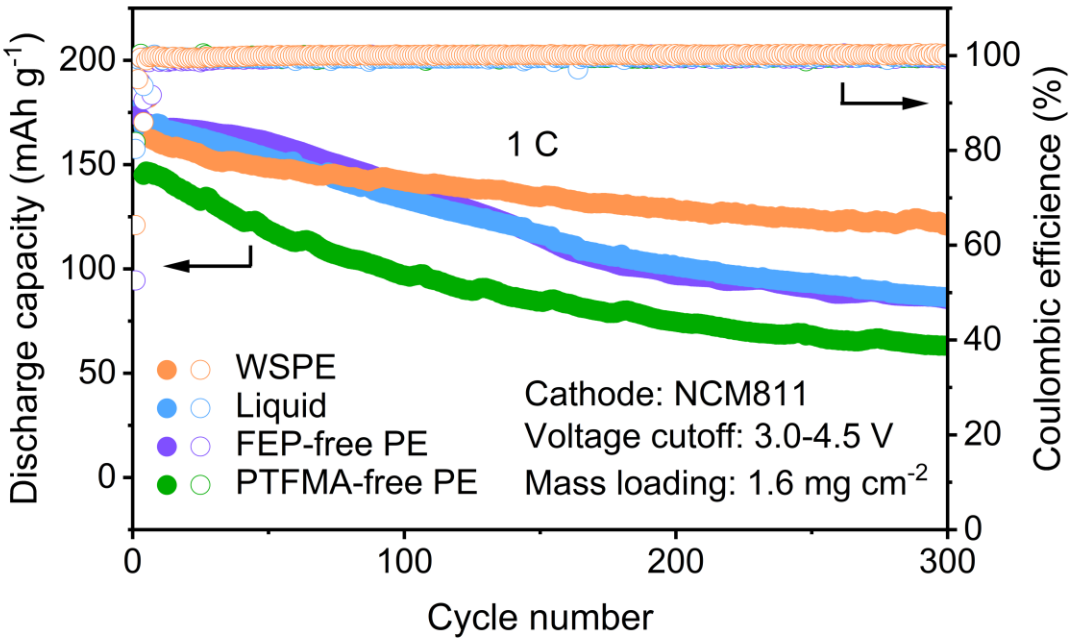

Fig. R10 (Supplementary Fig. 13 in revised Supplementary information). Cycling performance of Li/NCM811 cells using different electrolytes at 1 C between 3−4.5 V.

(3) The description of the composition and the preparation

The description of the composition and the preparation has been modified in the revised manuscript to ensure that the reader can fully understand, please see Paragraph 3, Page 5.

"TFMA monomer was used for in situ polymerization to form a brush-like PTFMA framework, and FEP was employed to act as a coupling agent, which formed unique dynamic non-bonding interactions with the short side chains of PTFMA to mimick the dynamic interactions of *Elodea densa* with water. A tiny amount of fluoroethylene carbonate (FEC) was added to optimize the interface and poly(ethylene glycol) diacrylate (PEGDA) was used as a cross-linking agent. The transparent WSPE was obtained by curing the precursor mixture at 70 °C for 5 h (Supplementary Fig. 2). The disappearance of C=C peak in FTIR suggests the successful polymerization occurred (Supplementary Fig. 3).[23,24] The perfluorinated materials used in this work benefit the electrochemical stability for the formation of fluorinated EEIs……" (Paragraph 3, Page 5)

(4) The interpretation on the bioinspiration

Learn from nature, our design is inspired by the perfect unity of natural biological structures and functionalities.

To present our design concept more clearly, we updated Fig. 1 in the revised manuscript (see Fig. R11 below). The inspiration from the water grass (*Elodea densa*) was raised from the integration of their structures and functions that have evolved over billions of years to adapt to the environment. *Elodea densa* has a unique structure that allows water to pass smoothly and maintain their structural integrity by the rapid swinging of their short lateral blades against strong currents. Meanwhile, the epidermal cell walls of *Elodea densa* are composed of hydrophilic polysaccharides which enhance the interaction of the blades with the water. This dynamic interaction forces *Elodea densa* to exhibit a stretched state in the water and doesn't impede water transport.

Inspired by the structure-function integration of *Elodea densa*, we designed a brush-like polymer with short side chains to reduce the transport resistance of Li^+ solvation clusters under current. More importantly, a Li^+ solvation cluster is constructed that allows it to form unique dynamic non-bonding interactions with the short side chains of polymer brushes, mimicking the dynamic interactions of *Elodea densa* with water. The strong interaction between the polymer framework and the coupling agent (FEP) not only ensures the stretching of the polymer chains, but also effectively induces a weak solvation structure (Fig. R11d). TFMA monomer was used for in situ polymerization to form a brush-like PTFMA framework, and FEP was coupled with the side chain of PTFMA. This double dipole coupling interaction successfully induced the generation of the weak solvation structure (Fig. R11e). Therefore, both high ion conductivity and easy desolvation would be achieved simultaneously and the operation temperature range can be expanded. The above discussion has been added in the manuscript to strengthen the description of our concept (Paragraph 1, Page 5).

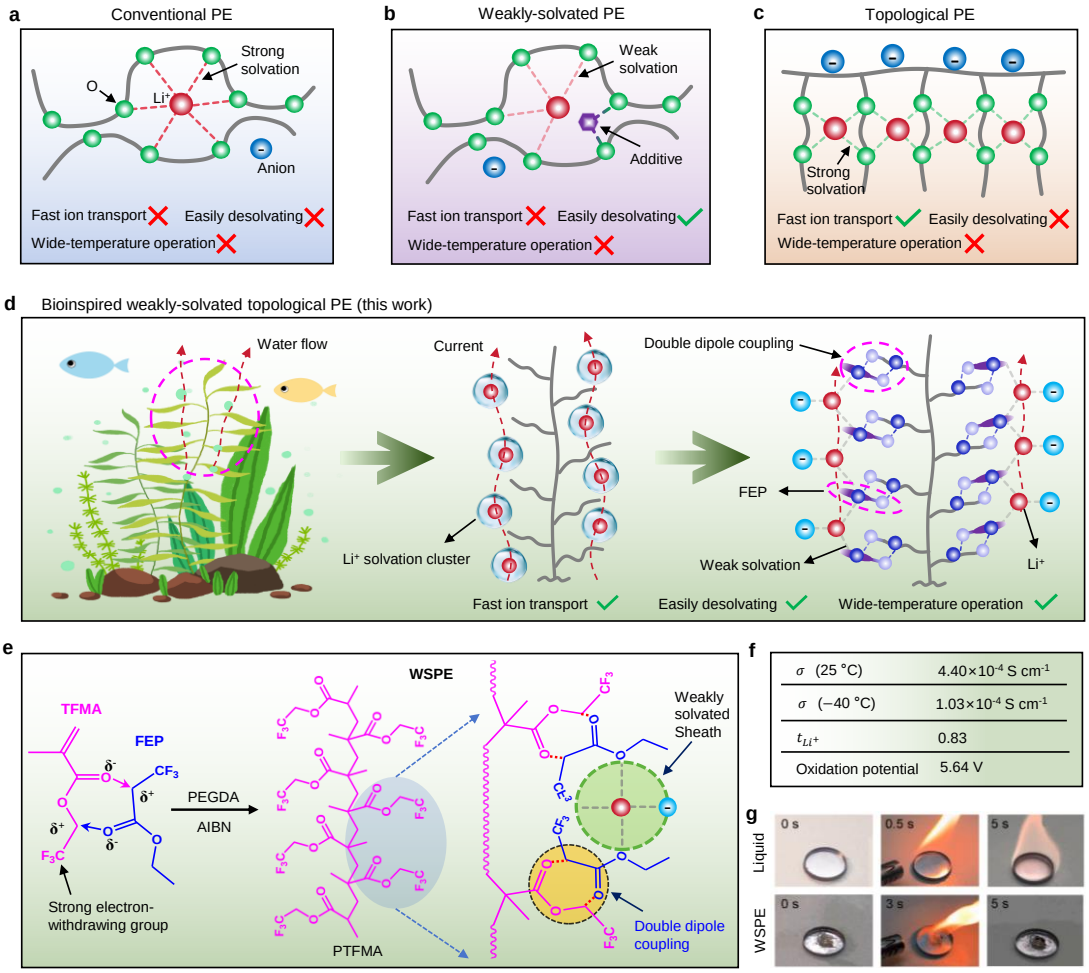

Fig. R11 Material design, fabrication, and properties of bioinspired weakly-solvated topological PE (Fig. 1 in revised manuscript)**.** (**a**) Conventional PE. (**b**) Weakly-solvated PE. (**c**) Topological PE. (**d**) Bioinspired weakly-solvated topological PE. (**e**) Structures and fabrication method of WSPE. (**f**) Electrochemical properties of WSPE. (**g**) Flame-retardant performance of WSPE.

To further validate the rationality of our concept, we conducted MD simulation. As shown in Fig. R12, the polymer PTFMA in this work has a brush-like configuration which is similar to that of *Elodea densa*. Meanwhile, the FEP molecules are inclined to accumulate around the polymer chains by a relatively high binding energy calculated by DFT (Table R1, Supplementary Table 1 in Supplementary information). As a result, the coupled structure of the FEP and PTFMA side chain regulates the solvation structure of the electrolyte for ultra-wide temperature lithium metal battery, showing the structure-function integration similar to *Elodea densa.* Fig. R12 has also been added in the revised Supplementary information as Supplementary Fig. 1.

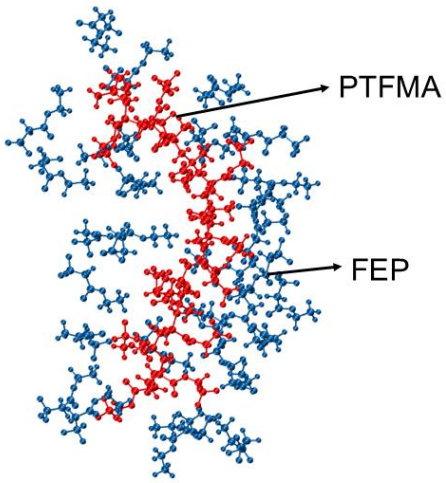

Fig. R2 (Supplementary Fig. 1 in revised Supplementary information). Snapshots of WSPE partial MD simulations.

Table R1. Binding energy between components in WSPE calculated by DFT.

Component A	Component B	Binding energy (kJ/mol)
$TFSI^-$	FEC	2727.87
$TFSI^-$	FEP	15645.06
$TFSI^-$	PTFMA	3346.05
PTFMA	FEC	7975.83
PTFMA	FEP	29380.90

Response to Reviewer #3:

1. Liu et al. demonstrated a functional polymer electrolyte with a concept of weakly solvation structure. Benefitting from its special structure, it shows promising behaviors over a wide temperature range. However, there is some concerns needs to be resolved prior to its publication. The concept of weakly solvating liquid electrolyte now becomes

common, while the weakly polymer electrolyte still seems fancy. The question is how to define the concept of weakly-solvated polymer electrolyte? What is superiority over the liquid electrolyte?

Response: Thank you very much for your useful comments.

(1) The weak solvation polymer electrolytes are those in which the coordination interaction of Li^+ is relatively weakened. For conventional weak solvation liquid electrolytes, they are usually prepared by adding weak solvents. For a weakly-solvated polymer electrolyte in this work, it is realized through a unique coordination regulation, i.e., a double dipole coupling interaction of the polymer framework with the solvent molecules. This interaction alters the electron cloud density distribution of the electrolyte to weaken the coordination to Li^+.

(2) The weak solvation polymer electrolyte combines the advantages of conventional weak solvation liquid electrolytes and polymer electrolytes. The microscopic coordination environments of Li^+ in weak solvation polymer electrolytes and weak solvation liquid electrolytes are similar. Thus, weak solvation polymer electrolytes inherit all the advantages of weak solvation liquid electrolytes over conventional liquid electrolytes, including low desolvation energy, inorganic-rich interfacial layers, and high-voltage stability. In addition, weak solvation polymer electrolytes own the advantages of traditional polymer electrolytes, such as safety and stability against Li metal. Moreover, the unique interactions in weak solvation polymer electrolytes result in a unique ion transport mechanism, which allows them to operate stably over a wide temperature range. In addition, a comparison of the battery performance of our electrolyte and weak solvation liquid electrolytes is shown in Table R1.

Table R1. The comparison of the battery performance of weak solvation polymer electrolyte and weak solvation liquid electrolytes.

Electrolyte type	Electrolyte formula	Cell type	Capacity retention at LT	Capacity retention at HT	Temperature range	Refs.
Weak solvation liquid electrolytes	LiFSI DME/TFEE (1.3 M; 2/8, v%) + 1% LiFMDFB + 0.05% $AgNO_3$	LCO/Li (3−4.4 V)	79.3%@300 cycles@0.2 C@−20 °C	−	−20−60 °C	12
	1M $LiPF_6$ in FEC: BTC (3:7 by volume)	NCM811/Li (2.5−4.7 V)	−	~80%@149 cycle@0.5 C@55 °C	−30−55 °C	13
	LiFSI-DME-TTE (1:1:3 by mol)	LCO/Li (3–4.5 V)	88%@1 cycle@0.15 C@ −30 °C (charged at RT)	81.3%@200 cycles@0.7 C@55 °C	−30−55 °C	14
	LHCE-LiTD55	NCM523/Li	71%@1 cycle@0.1 C@−40 °C	80%@200 cycles @80 °C	−40−80 °C	15
This work	WSPE	NCM811/Li (3−4.3 V)	97.1%@200cycles @0.2 C@−20 °C	94%@100cycles@1 C@80 °C	−30−80 °C	

2. The polymer electrolyte is initiated by a polymerization process. I have a significant concern on the liquid residue within the polymer? The amount of liquid residue could considerably strength the ionic transfer and interface stability, however not belongs to the definition of polymer electrolyte. Please clarify the issues.

Response: Thank you very much for your comments.

Polymer electrolytes can be classified as all solid polymer electrolytes (SPEs) and gel polymer electrolytes (GPEs).[16,17] In comparison, GPEs can solve the problem of battery leakage and maintain high ionic conductivity. Even in traditional polymer electrolytes, such as PVDF, ion transport is achieved by the residual DMF solvent in them.

Herein, the weak solvation polymer electrolyte (WSPE) was prepared by the liquid electrolyte (1M LiTFSI in FEP), a small amount of FEC additives as well as TFMA and PEGDA monomers by in-situ polymerization. The disappearance of the C=C peak in FTIR indicates the complete polymerization of TFMA and PEGDA precursors (Fig. R1, Supplementary Fig. 3 in Supplementary information). FEP, meanwhile, is bound to the

polymer framework PTFMA through the strong double dipole coupling interactions (Table R2, Supplementary Table 1 in Supplementary information).

More interestingly, the unique double dipole coupling interaction between the FEP and PTFMA framework induces the generation of the weak solvation structure. This allows the polymer matrix to play a more important role in regulating the electrochemical performance of the electrolyte, rather than just enhancing safety in the traditional sense. Therefore, the WSPE is a unique polymer electrolyte which is significantly different with conventional polymer electrolytes.

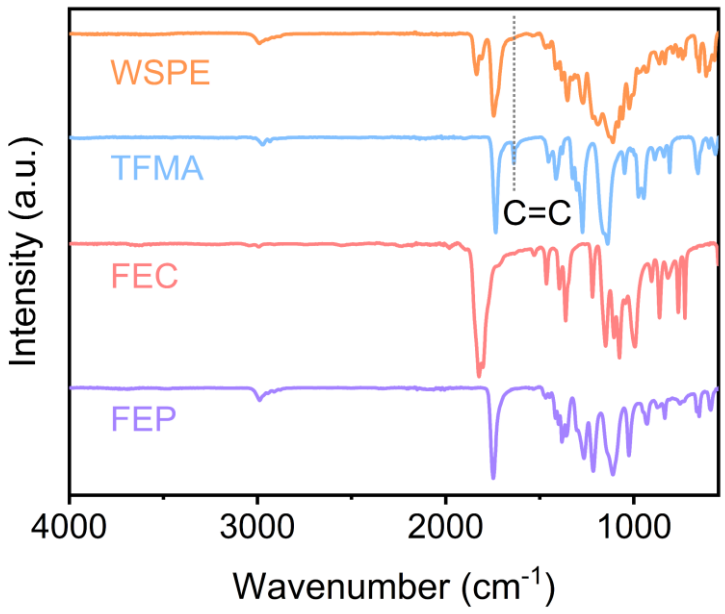

Fig. R1. FTIR spectra of FEP, FEC, TFMA and WSPE.

Table R2. Binding energy between components in WSPE calculated by DFT.

Component A	Component B	Binding energy (kJ/mol)
$TFSI^-$	FEC	2727.87
$TFSI^-$	FEP	15645.06
$TFSI^-$	PTFMA	3346.05
PTFMA	FEC	7975.83
PTFMA	FEP	29380.90

3. How about the ionic transport mechanism in the polymer electrolyte? The unique transfer mechanism is suggested to compare with the classic PEO and PVDF polymer electrolyte.

Response: Thank you very much for your helpful comments.

As compared to classical PEO and PVDF polymer electrolytes, the unique ion transport mechanism of our electrolyte is described as follows: Firstly, in the PEO polymer electrolyte, Li^+ is coordinated with the O atoms of the PEO, and ion transport is realized by the movement of the chain segments of the PEO. Thus, the ion transport rate is completely dependent on the chain segment motion, and the ionic conductivity has high temperature dependence.[7] The PVDF polymer itself has no lithium salt dissociation ability, so the Li^+ transport in the PVDF polymer mainly relies on the small amount of DMF solvent residual in the PVDF.[18] While this transport allows for high ionic conductivity, the $[Li(DMF)_x]^+$ clusters, which are capable of rapid migration, directly lead to an unstable interfacial layer dominated by DMF decomposition products. Moreover, the porous structure of the PVDF polymer matrix would cause uneven current and ion transport on the surface of the Li anode, which is very likely to lead to rapid growth of Li dendrites and short circuit of the battery.[19]

Different from those reported in typical PEO and PVDF polymer electrolyte, our design focuses on a unique double dipole coupling interaction between polymer framework and the FEP molecules, resulting in the formation of anion-dominated Li^+ weak solvation clusters. On the one hand, Li^+ transport is cluster-based and does not depend entirely on the movement of the polymer chain segments. On the other hand, there is a dynamic interaction between the PTFMA framework and the FEP at the periphery of the Li^+ solvation clusters. Therefore, Li^+ clusters can realize rapid transport along the framework through the constant coupling and uncoupling of peripheral FEP molecules with the PTFMA. In addition, Li^+ weak solvation clusters induced the formation of inorganic-rich interfacial phases. In summary, this unique transport mechanism brings in a high room temperature ionic conductivity and an optimized interfacial layer.

4. Continue to the last question, how about the ion diffusion mechanism within the cathode, especially with thick cathode?

Response: Thank you very much for your valuable comments.

Unlike conventional polymer electrolytes prepared by ex-situ methods, we used in-situ polymerization to prepare WSPE. Therefore, the small molecule precursors can fully penetrate into the pores of the cathode prior to polymerization. After polymerization, WSPE can be tightly wrapped around the surface of the cathode particles, as shown in Figs. R2a, b. As a comparison, the pristine NCM811 itself presents uncoated particles as well as pores in the images of electrodes (Figs. R2c, d). Compared with ex-situ polymerization, in-situ polymerization can effectively reduce the interfacial contact resistance between electrolyte and cathode, especially for thick cathode, because the capacity of thick cathode can be fully performed by using this approach.

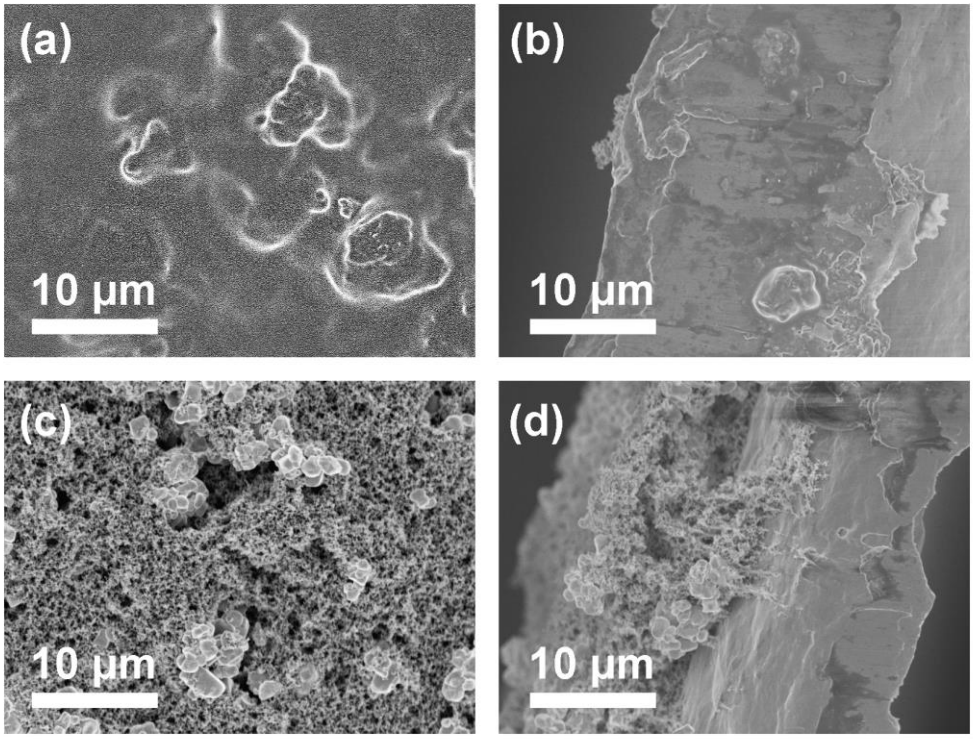

Fig. R2. (a) Surface and (b) cross-sectional SEM images of in situ polymerized NCM811 electrodes. (c) Surface and (d) cross-sectional SEM images of pristine NCM811 electrodes.

5. Despite the beauty of figure drawing, I have some concerns on the scientific aspects on this work. Lots of important electrochemical issues has been neglected, such as the cathode loading, the galvanic discharge/charge protocol (with the cutoff conditions).

Some important parameters are suggested to added into the figures, but not just simply listing the rate of 1C, 2C. The cycling rate has no any meaning if there is no other parameters. Same to Figure 5a without no any information about its current density and areal capacity.

Response: Thank you very much for your valuable suggestion.

According to your suggestion, we have added these parameters to the figures that relate to the performance of the cells. The current density and surface capacity information in Fig. 5a is also added in the revised manuscript.

6. What is the reason for the fire resistance shown in Figure 1g? The polymer electrolyte seems also flame until its fully collapsed. Is it due to the combustion of residue liquid electrolyte within the polymer electrolyte?

Response: Thank you very much for your helpful comments. Sorry for not describing it clearly.

Generally, the fluoropolymers have good flame-retardant properties. The F radicals released from fluoropolymers at high temperatures can capture the H•/HO• radicals generated during combustion. The capturing of free radicals by F atoms would inhibit the dehydrogenation reaction of polymers during degradation and promotes the dehydrofluorination reaction, thus facilitating the generation of carbonaceous products. The product has a stable aromatic structure and is not easily oxidized by oxygen, thus forming a dense char layer on the surface of the polymer, blocking heat and oxygen, and performing a flame-retardant function.[20,21] The similar phenomenon has been detected in our system. As shown in Fig. R3, the WSPE was ignited after 3s of continuous flame contact with only a small spark. Rapid self-extinguishing was achieved after removing the flame for 2 s. A charcoal layer on the polymer surface could be observed. As a contrast, the liquid electrolyte ignites when it comes into contact with the flame for only 0.5 s and continues to burn after the flame is removed until the electrolyte is exhausted.

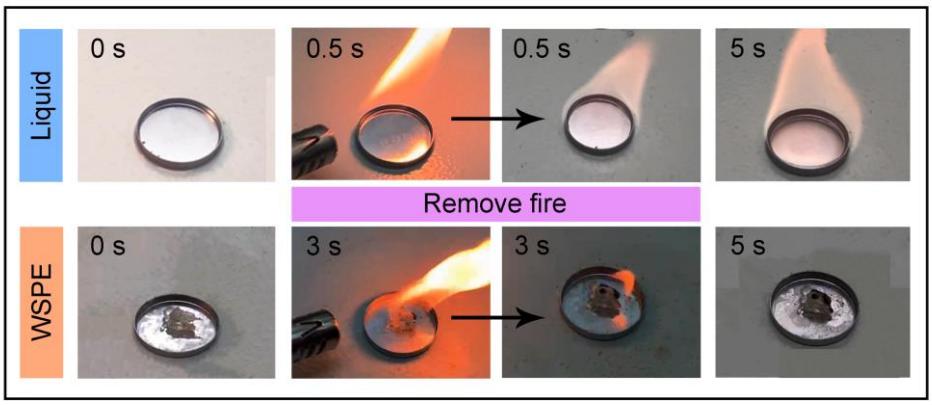

Fig. R3. The flame-retardant performance of liquid electrolyte and WSPE.

7. Will this solvation structure change under extreme temperatures? Does the desolvation process differ at various temperatures?

Response: Thank you very much for your constructive comments.

(1) The changes in solvation structure are inevitable as temperature changes. However, based on the interfacial impedance at different temperatures in Figs. 3c, d and the excellent high and low temperature cycling performance in Figs. 3e-g, we speculate that the change of solvation structure in our electrolyte is insignificant in response to the temperature, i.e., the electrolyte system exhibits a weak solvation structure even under extreme temperatures. To confirm this speculation, we used MD simulations to analyze the solvation structure of WSPE at different temperatures (Fig. R4). As shown in Fig. R4a, the position of the solvation sheath around Li^+ changes hardly with temperature. There is only a relative increase or decrease in the number of particles, implies that the size of the Li^+ solvation clusters does not change significantly. Figs. R4b-d demonstrate the variation of coordination number (CN) of each component with temperature. It can be seen that the CN of FEP and FEC molecules gradually increases and the CN of $TFSI^-$ gradually decreases with decreasing temperature. That is, the number of solvent molecules in the first Li^+ solvation sheath increases while the number of $TFSI^-$ decreases with decreasing temperature. However, even at −30 °C, the CNs of FEP, FEC and $TFSI^-$ at a distance of 3.0 Å from Li^+ were 1.8, 0.5 and 3.2, respectively. That means the number of $TFSI^-$ in the first Li^+ solvation sheath is still higher than that of solvent molecules, i.e., the anion-dominated weak solvation

structure is maintained in WSPE at −30 °C. In conclusion, the solvation structure of WSPE exhibits a very low temperature dependence, which is a key point for its excellent performance in extreme temperature environments.

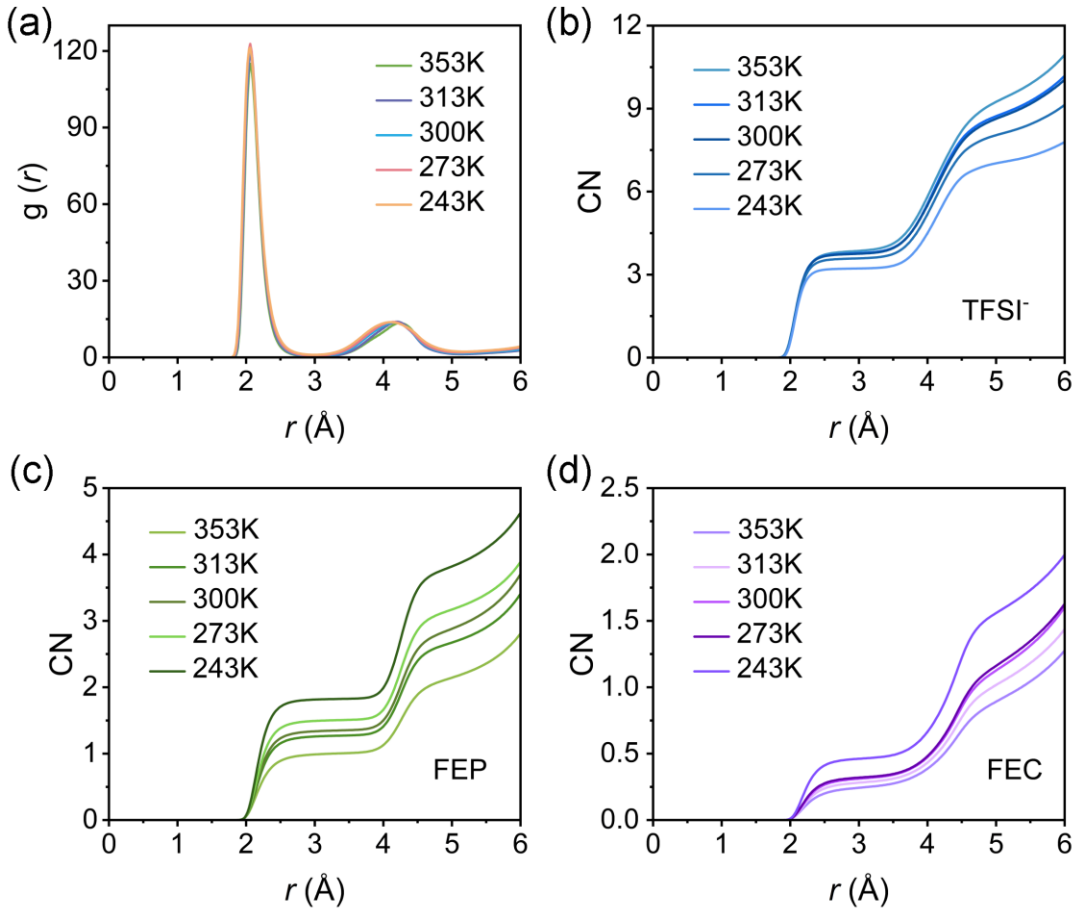

Fig. R4. (a) The RDF of Li^+ in WSPE under different temperatures. The CNs of Li^+ with (b) $TFSI^-$, (c) FEP and (d) FEC in WSPE at different temperatures.

(2) The temperature change does not lead to a change in the desolvation process and that the desolvation energy increases slightly with decreasing temperature. Indeed, the electrode/electrolyte interface reaction is known to occur through the following mechanisms. During the charging process, Li^+ is stripped from the solvation clusters that surround it while adsorbing to the SEI surface (desolvation process). Subsequently, the Li^+ migrate to the Li surface via the SEI and undergo an electron transfer reaction (charge transfer process). These reactions occur in reverse during discharge.[22] The solvation structure of Li^+ in our electrolyte system does not change distinctly with temperature, and therefore the desolvation process does not change correspondingly. The desolvation energy is determined by the coordination structure of Li^+. The Li^+

solvation sheath consists of solvent molecules and anions. Generally, the interactions of Li^+-anions on the Li^+ desolvation at the interface can be neglected for the electrostatic repulsion of the anions on the electrode surface.[23] Therefore, based on the fact that the CN of solvent molecules in the first Li^+ solvation sheath increases relatively with decreasing temperature, it is known that the desolvation energy will increase slightly.

8. Lots of supplementary details needs to be provided on the large pouch cell, especially 5 Ah pouch cell, for instance, picture before and after assembly, digital picture of assembly process, the pouch cell after cycling. I have a huge concern on the assembly of such high areal high capacity pouch cell, in comparison with liquid electrolytes.

Response: Thank you very much for your constructive suggestion.

According to your suggestion, the assemble process as well as the details of the 5.4 Ah pouch cell are as below (Fig. R5):

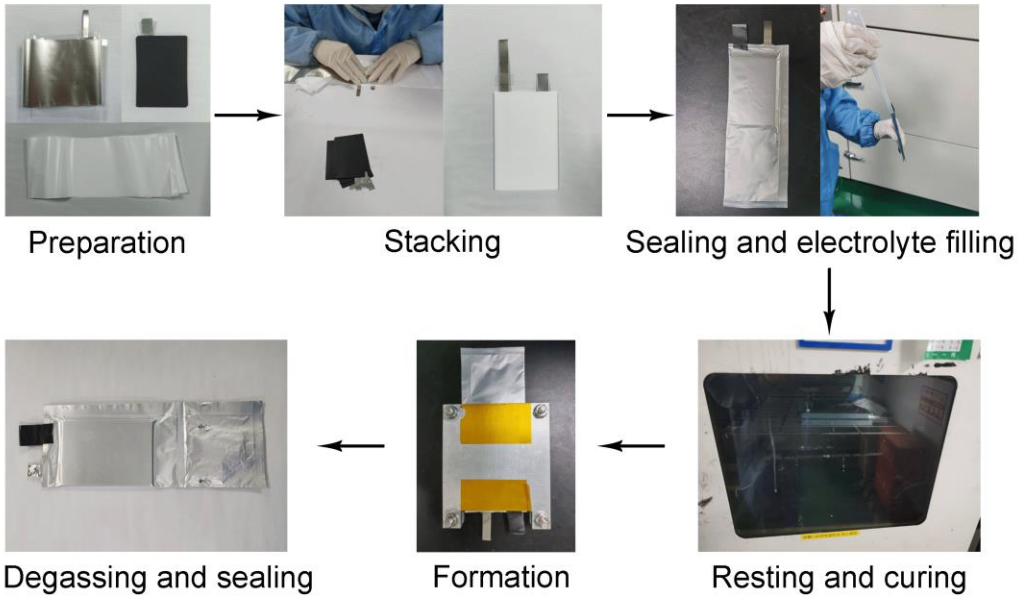

Fig. R5 (Supplementary Fig. 29 in revised Supplementary information). Diagram of the preparation process of the 5.4 Ah pouch cell.

Preparation: The rolled cathode sheet (active materials mass loading of 24.02 mg cm^{-2}) was slit into 5 cm×8 cm rectangles, and the Li foils with a thickness of 50 μm as well as polypropylene separator with a thickness of 16 μm were prepared;

Stacking: Stack the cathode, separator, and anode layer by layer to get a jelly roll. Weld the tabs on the stacked jelly roll;

Sealing: Sealing the welded jelly roll in the aluminum laminated plastic film. In addition to the body of the jelly roll, the aluminum laminated plastic film leaves a residual volume, which is called the gas pouch and is used to collect the gas generated during the formation process of the jelly roll;

Electrolyte filling: The aluminum laminated plastic film is opened and the electrolyte precursor is injected into the jelly roll and sealed;

Resting and curing: The cells were rested at room temperature for 24 h to ensure that the injected electrolyte precursor fully impregnated the electrode. The liquid precursor is then cured by heating at 70 ℃ for 12 h under pressure.

Formation: The pouch cell was first charged to 4.3 V at constant current at a small current of 0.25 A, stood for 10 min, and then discharged to 3.8 V. The charge/discharge curves of the formation process are shown in Fig. R6. The formation process is performed under pressure.

Degassing and sealing: The gas pouch is punctured and vacuumed, then sealing is performed along the jelly roll.

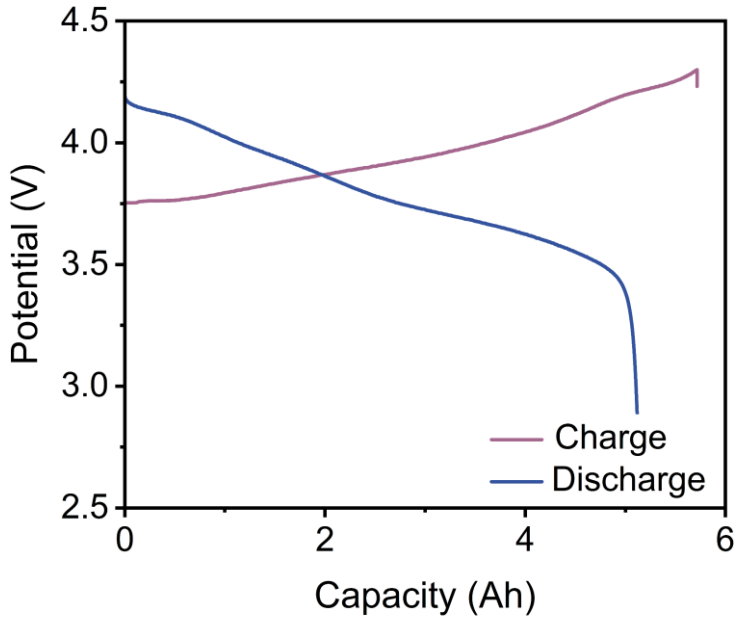

Fig.R6. Charge-discharge curves of the pouch cell with designed capacity of 5.4 Ah.

The detailed parameters of the 5.4 Ah pouch cell are shown in Table R3. These details have been added in the revised Supplementary information as Supplementary Fig. 29.

Table R3. Parameters of the 5.4 Ah pouch cell.

	Thickness (μm)	Areal weight (mg cm^{-2})	Layers	Width (cm)
Li anode	50	2.67	15	8.2
NCM811 cathode	70	24.02	14	8
Separator	16	1.32	16	8.7
Electrolyte	2 g Ah^{-1}			
Total weight (g)	43.16			
Discharge capacity (Ah)	5.124			
Voltage (V)	3.8			
Energy density (Wh kg^{-1})	451			

The liquid precursor of the electrolyte undergoes sufficient activation prior to thermal polymerization to ensure that the liquid precursor can infiltrate the positive electrode and achieve excellent pouch cell performance. Therefore, our electrolytes are fully comparable to liquid electrolytes.

References

1. Zou, Y. et al. Non - flammable electrolyte enables high - voltage and wide - temperature lithium - ion batteries with fast charging. *Angew. Chem. Int. Ed*. **135**, e202216189 (2023).
2. Zhou, G., Yu, J. & Ciucci, F. In situ prepared all-fluorinated polymer electrolyte for energy-dense high-voltage lithium-metal batteries. *Energy Storage Mater*. **55**, 642-651 (2023).
3. Li, Y. et al. Hexagonal boron nitride induces anion trapping in a polyethylene oxide based solid polymer electrolyte for lithium dendrite inhibition. *J. Mater. Chem. A*. **8**, 9579–9589 (2020).

4. Liu, Q. et al. Transference number reinforced-based gel copolymer electrolyte for dendrite-free lithium metal batteries. *ACS Appl. Mater*. *Interfaces.* **14**, 26612-26621 (2022).
5. Zhang, W., Yang, T., Liao, X., Song, Y. & Zhao, Y. All-fluorinated electrolyte directly tuned Li^+ solvation sheath enabling high-quality passivated interfaces for robust Li metal battery under high voltage operation. *Energy Storage Mater.* **57**, 249–259 (2023).
6. Atik, J. et al. Cation-assisted lithium-ion transport for high-performance PEO-based ternary solid polymer electrolytes. *Angew. Chem. Int. Ed*. **60**, 11919–11927 (2021).
7. Hu, A. et al. Ion transport kinetics in low-temperature lithium metal batteries. *Adv. Energy Mater*. **12**, 2202432 (2022).
8. Kim, S. C. et al. High-entropy electrolytes for practical lithium metal batteries. *Nat. Energy.* **8**, 814–826 (2023).
9. Jiang, X. et al. Breaking solvation dominance of phosphate via dipole–dipole chemistry in gel polymer electrolyte. *ACS Energy Lett.* **9**, 3369–3379 (2024).
10. Weng, S. et al. Temperature-dependent interphase formation and Li^+ transport in lithium metal batteries. *Nat. Commun.* **14**, 4474 (2023).
11. Kang, C. et al. Low-solvent-coordination solvation structure for lithium-metal batteries via electric dipole-dipole interaction. *Angew. Chem. Int. Ed*. e202412703 (2024).
12. Kim, S. et al. Wide-temperature-range operation of lithium-metal batteries using partially and weakly solvating liquid electrolytes. *Energy Environ. Sci*. **16**, 5108–5122 (2023).
13. Xiao, P. et al. A nonflammable electrolyte for ultrahigh-voltage (4.8 V-class) Li||NCM811 cells with a wide temperature range of 100 °C. *Energy Environ. Sci*. **15**, 2435-2444 (2022).
14. Ren, X. et al. Designing advanced in situ electrode/electrolyte interphases for wide temperature operation of 4.5 V Li||$LiCoO_2$ batteries. *Adv. Mater.* **32**, 2004898 (2020).

15. Li, J. Mild and controllable solid electrolyte interphase formation for high-voltage lithium metal batteries in a wide-temperature range from −40 °C to 80 °C. *Chem. Eng. J.* **452**, 139398 (2023).
16. Long, L. Polymer electrolytes for lithium polymer batteries. *J. Mater. Chem. A*. **4**, 10038-10069 (2016).
17. Wu, Y. Advances and prospects of PVDF based polymer electrolytes. *J. Energy Chem*. **64**, 62-84 (2022).
18. Huang, Y. et al. Conformational regulation of dielectric poly(vinylidene fluoride)-based solid-state electrolytes for efficient lithium salt dissociation and lithium-ion transportation. *Adv. Energy Mater*. **13**, 2203888 (2023).
19. Yang, W. et al. Solvation-tailored PVDF-based solid-state electrolyte for high-voltage lithium metal batteries. *Angew. Chem. Int. Ed*. **136**, e202401428 (2024).
20. Wu, M. Fire-safe polymer electrolyte strategies for lithium batteries. *Energy Storage Mater.* 103174 (2024).
21. Hu, A. et al. Nonflammable polyfluorides-anchored quasi-solid electrolytes for ultra-safe anode-free lithium pouch cells without thermal runaway. *Adv. Mater.* **35**, 2304762 (2023).
22. Zhang, J.-W. Tuning solvation structure to enhance low temperature kinetics of lithium-ion batteries. *Energy Storage Mater.* 103698 (2024).
23. Ma, T. et al. Optimize lithium deposition at low temperature by weakly solvating power solvent. *Angew. Chem. Int. Ed.* **61**, e202207927 (2022).

Response to Reviewer #4:

The manuscript entitled “Bioinspired topological polymer electrolyte for ultra-wide temperature lithium metal battery” co-authored by Shuohan Liu, Wensheng Tian, Jieqing Shen, Zhikai Wang, Hui Pan, Xuchen Kuang, Cheng Yang, Shunwei Chen, Xiujun Han, Hengdao Quan, and Shenmin Zhu presents an interesting study on a 1 M LiTFSI FEP + 5 wt% FEC embedded in a PTFMA matrix electrolyte. The originality of this manuscript lies in the selection of FEP and PTFMA which present an asymmetrical structure that induces double dipole interaction. This unique configuration seems to form a weak solvation structure that offers fast and uniform Li+ deposition and stable electrolyte-electrode interfaces at extreme temperatures. Remarkable performances are demonstrated. However, the present revised manuscript lack in explaining the intrinsic reason and mechanism leading to such remarkable performances. Furthermore, this manuscript defines the WSPE as a separate category from GPE. However, this material being a liquid electrolyte (LE) trapped in a polymer matrix is in fact a GPE, so it is better not to create an unnecessary category. In addition, the analogy with Elodea densa is not helpful for reader and rather confusing. The is the main misleading point as this algae is as a solid-like structure in water whereas the design material is a fluorinated gel electrolyte not a solid. Indeed, no mechanical/viscosity characterization are provided. Thanks to the originality but due to lack of clearness in the discussion, we recommend this manuscript to be accepted but after some major changes.
We have couple of comments thus to address as listed below:

1. The comparison with the algae would make sense if the polymer matrix would stretch like the leaves in water which is useless for the present work. In addition, other publications already exists for GPE with branched polymer matrix. (e.g. https://doi.org/10.1016/j.ssi.2016.05.019)

Response: Thank you very much for your valuable comments.

You mentioned that some publications have already reported on GPE with a branched polymer matrix. However, this work focuses on designing and constructing the interaction between the polymer framework and liquid to generate a weak solvation structure in the GPE, rather than on the fabrication of a branched polymer matrix for

GPE. Therefore, the concept of bioinspiration in this work is an analogy on the interactions between materials — water grass with water *vs.* polymer framework with liquid electrolyte, beyond the structure mimicking of water grass. Unlike terrestrial plants having hydrophobic wax layer on leaf surface, the epidermal cell walls of water grass are hydrophilic composed of polysaccharides, which enhance the interaction of the blades with the water to adapt to aqueous environment. We choose FEP with an asymmetric structure to the polymer side chain to form unique dynamic non-bonding interactions with the branched polymer, thereby mimicking the dynamic interactions between water and water grass. The short side chains of the branched polymer provide interaction sites with FEP, enabling regulation on the solvation structure.

To clarify our design concept and avoid confusion, we have modified the description accordingly, and made it more tersely and clearly. Also, the reference you mentioned has been cited as Ref. 21 in the revised manuscript. We hope that our response will satisfy you.

2. A GPE is a LE embedded in a polymer matrix. From the experimental section it seems that the electrolyte composition is about 65 wt.% of solvent (FEC + FEP) and the rest is LiTFSI salt 13.5 wt.%, PTFMA polymer 20 wt.%, crosslinker 1wt.%, and initiator 0.5 wt.%. Therefore, the electrolyte is a GPE not a new class of electrolyte. Please adjust the manuscript title and text accordingly. A proposition: weakly solvated gel polymer electrolyte (WSGPE).

Response: We appreciate and agree with you on the definition of our materials. As you suggested, we have replaced polymer electrolyte by weakly solvated gel polymer electrolyte (WSGPE) in title and text in the revised manuscript.

3. How does the PEGDA interact with the polymer matrix? Is there any remaining PEGDA in the system?

Response: Thank you for your comments. During the polymerization process, a small amount of PEGDA (1 wt.%) acted as cross-linking agent, converting the polymer matrix into cross-linked network. No residual PEGDA was detected in the system, indicated by the disappearance of the C=C peak in the FTIR spectra (Fig. R1).

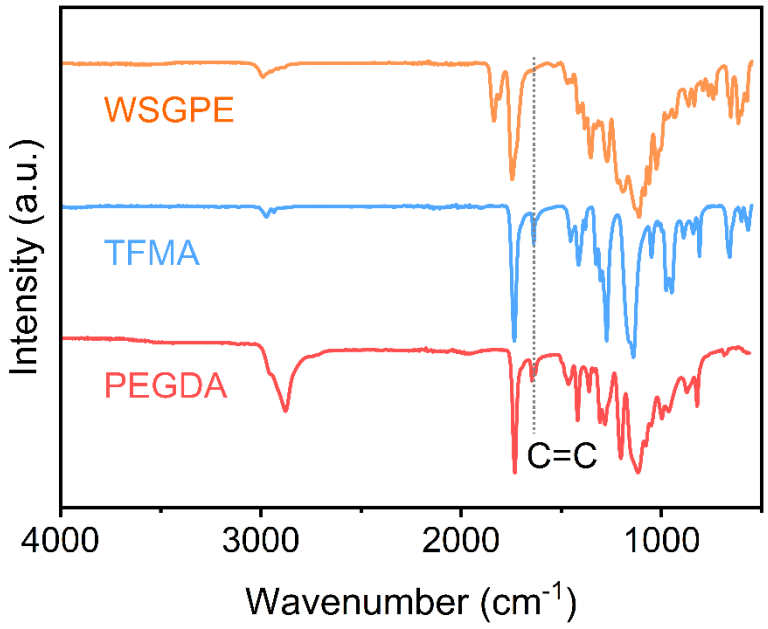

Fig. R1. FTIR spectra of PEGDA, TFMA and WSGPE. The characteristic peak representing C=C disappeared in WSGPE.

4. Page 3 line 8 is grammatically wrong.

Response: The grammar has been corrected and yellow highlighted in the revised manuscript. Also, we have carefully checked the entire text.

5. Previous work on PTFMA should be cited: https://doi.org/10.1016/j.jpowsour.2024.235189 doi/abs/10.1002/cnma.202400180, https://doi.org/10.1002/eem2.12351.

Response: The recommended references have been cited as Refs. 23, 24 in the revised manuscript.

6. Previous work of FEP should be cited: https://www.nature.com/articles/s41467-023-36853-x.

Response: We have cited the reference as Ref. 12 in the revised manuscript to support

our discussion.

7. There is not much explanation on the effect of FEC which is unclear in the text. So, does the materials behave the same without FEC in its formulation. What is the corresponding volume fraction? What about diffusivity of FEC and the possibility to coordinate cation or anion and participate in the ionic transport? This could explain the high conductivity even at low temperature. In addition, is there degradation of FEC with Li metal to promote a stable SEI? In short, it is important to decorrelate the effect of FEC from the gel electrolyte.

Response: Thank you for your comments.

The volume fraction of FEC in WSGPE is approximately 5 vol.%. To investigate the effect of FEC, we prepared a FEC-free gel polymer electrolyte (FEC-free GPE) by replacing FEC with an equal mass of FEP. The radial distribution function (RDF) and the corresponding coordination number (CN) in FEC-free GPE are simulated, as shown in Fig. R2. In RDF, the initial peaks corresponding to Li^+–O ($TFSI^-$) and Li^+–O (FEP) appear at 2.04 Å and 2.12 Å, respectively, which are nearly identical to those in WSGPE, where the initial peaks for Li^+–O ($TFSI^-$) and Li^+–O (FEP) are observed at 2.06 Å and 2.12 Å, respectively (Fig. R3). At a distance of 3.0 Å, the CNs of FEP and $TFSI^-$ are 1.54 and 3.74, respectively (the CN ratio of $TFSI^-$ to solvent molecule is 2.4, which is also highly consistent with 2.3 in WSGPE). The results indicate that FEC has no distinct effect on the solvation structure of WSGPE.

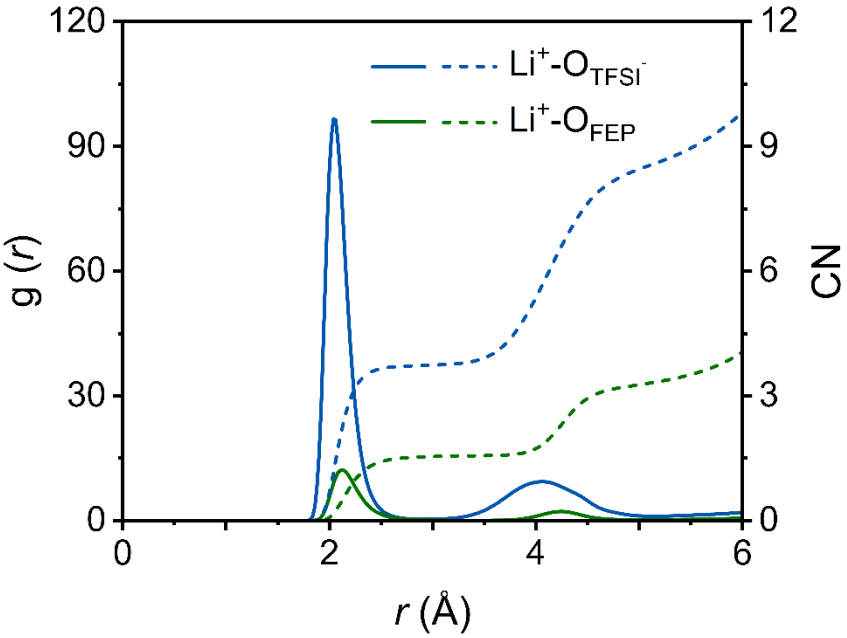

Fig. R2. RDFs and CNs of Li^+ in the FEC-free GPE.

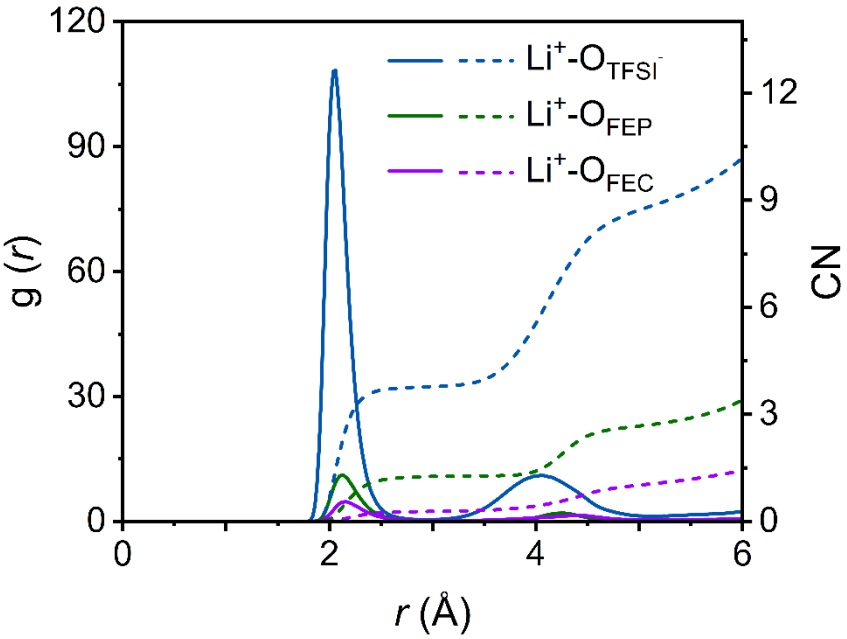

Fig. R3. RDFs and CNs of Li^+ in the WSGPE.

FEC in WSGPE exhibits a high diffusion coefficient of 2.33×10^{-10} m^2 s^{-1}. However, FEC is weak in coordinating with both Li^+ and $TFSI^-$ (Fig. R3 and Table R1), and thus has a minimal effect on ion transport. As shown in Fig. R4, the diffusion coefficients of Li^+ and $TFSI^-$ in FEC-free GPE are 1.55×10^{-11} and 1.72×10^{-11} m^2 s^{-1},

respectively, no obvious difference with that in WSGPE (the diffusion coefficients of Li^+ and $TFSI^-$ are 1.56×10^{-11} and 1.66×10^{-11} m^2 s^{-1}, respectively). The ionic conductivities of WSGPE and FEC-free GPE at room temperature are 4.4×10^{-4} and 4.1×10^{-4} S cm^{-1}, respectively, which are almost the same (Fig. R5). This further confirms the minimal effect of FEC on ion transport. The ionic conductivities of WSGPE and FEC-free GPE are 1.03×10^{-4} and 9.30×10^{-5} S cm^{-1} at −40°C, respectively (Fig. R6). This difference can be attributed to the enhanced coordination of Li^+ by FEC at such low temperature, which allows FEC to facilitate ion transport to a certain extent, as revealed by the simulation results in Fig. R7d. It is worth mentioning that there is still a weak solvation structure in WSGPE even at low temperature of −30°C, and the coordination of ions by FEC remains relatively weak, limiting its contribution to ion transport (Fig. R7). Thus, it is reasonable to imply that the high ionic conductivity of WSGPE at low temperatures is primarily attributed to the framework-induced weak solvation structure.

Table R1. Binding energy between components in WSGPE calculated by DFT.

Component A	Component B	Binding energy (kJ/mol)
$TFSI^-$	FEC	2727.87
$TFSI^-$	FEP	15645.06
$TFSI^-$	PTFMA	3346.05
PTFMA	FEC	7975.83
PTFMA	FEP	29380.90

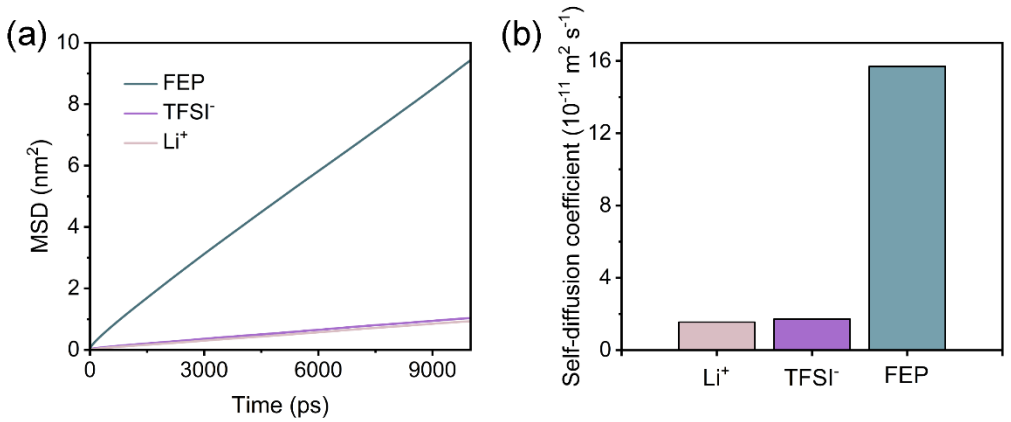

Fig. R4. (a) MSD-time curves and (b) the corresponding diffusion coefficients of FEC-free GPE components.

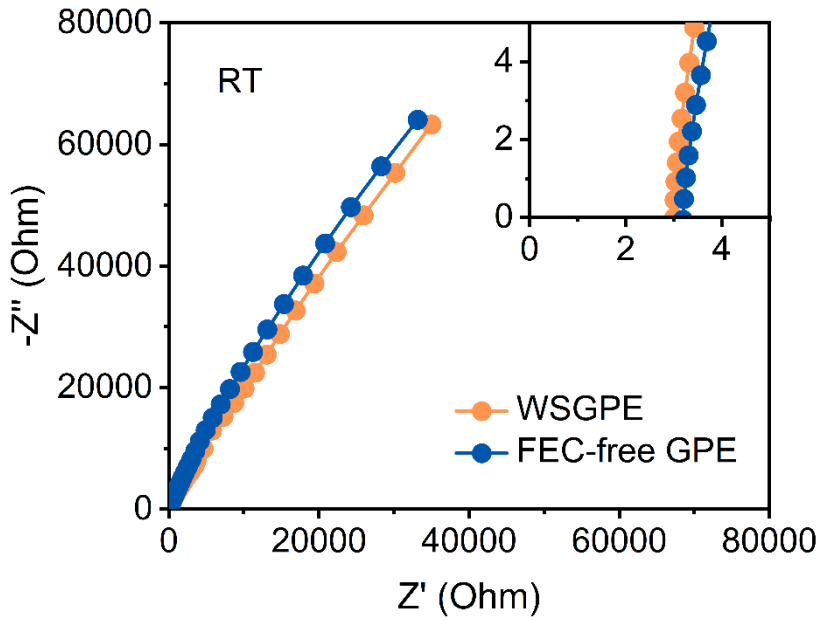

Fig. R5. Nyquist curves of the SS/WSGPE/SS and SS/FEC-free GPE/SS cells at room temperature.

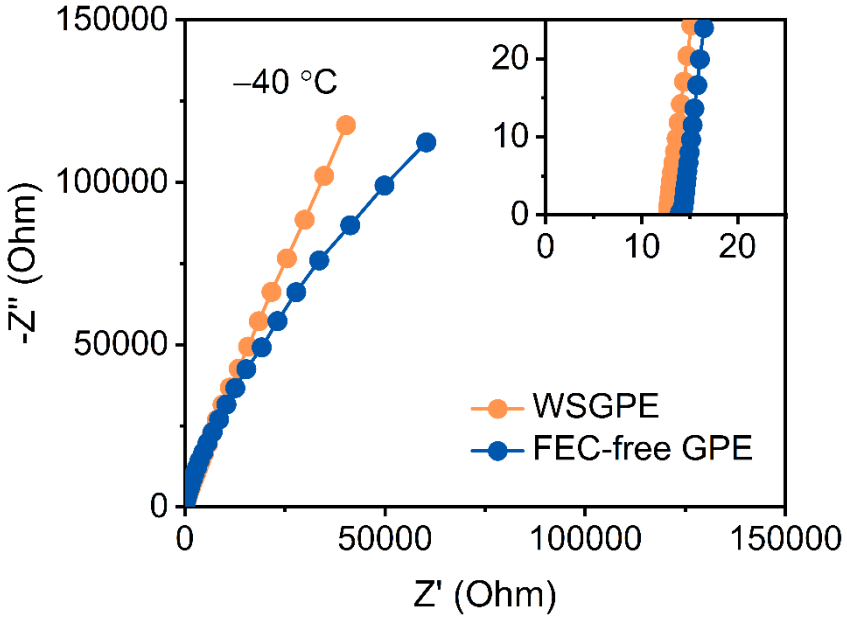

Fig. R6. Nyquist curves of the SS/WSGPE/SS and SS/FEC-free GPE/SS cells at −40°C.

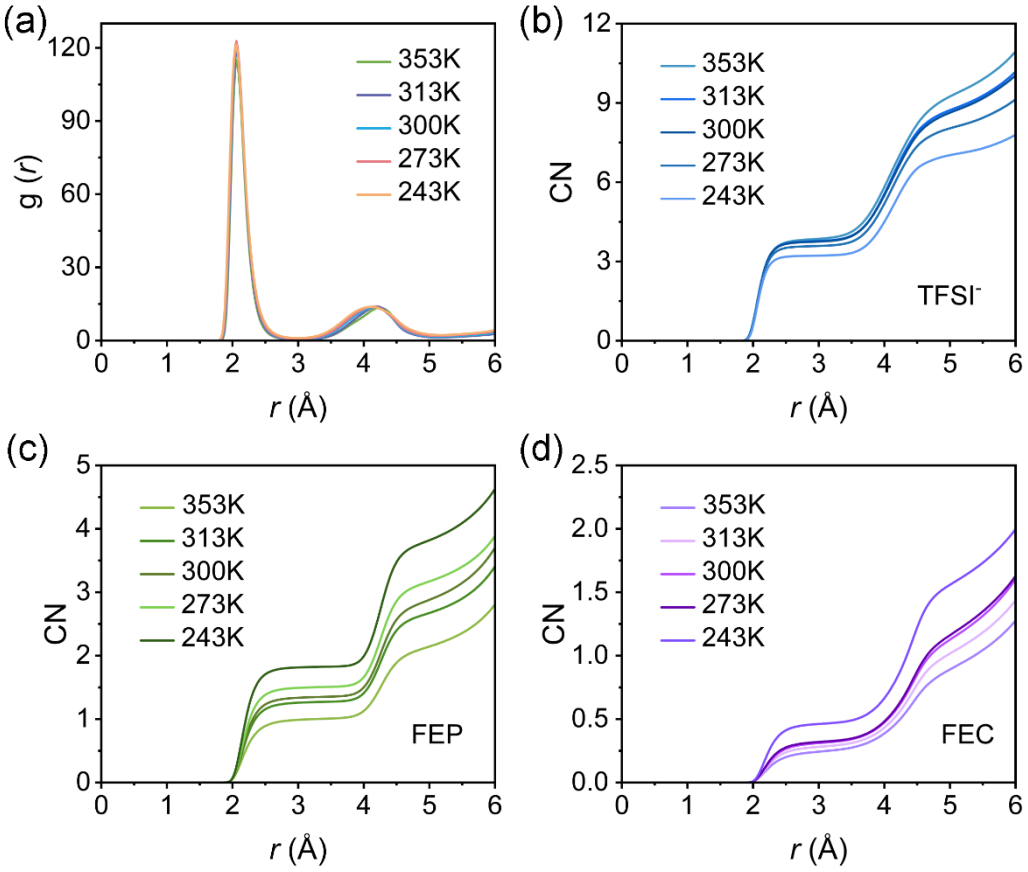

Fig. R7. (a) The RDF of Li^+ in WSGPE under different temperatures. The CNs of Li^+ with (b) $TFSI^-$, (c) FEP and (d) FEC in WSGPE at different temperatures.

Similar to other reports, FEC is used as a film-forming additive in WSGPE to promote the formation of a stable SEI layer.[1-3] Under a current density of 0.5 mA cm^{-2} and an area capacity of 0.5 mAh cm^{-2}, the Li/FEC-free GPE/Li cell exhibits an average unilateral overpotential of over 150 mV (Fig. R8), whereas the Li/WSGPE/Li cell shows only about 60 mV (Fig. R9). The EIS spectra of Li symmetric cells assembled with different electrolytes after 100 cycles are compared in Fig. R10, indicating that the presence of FEC would significantly reduce the interfacial impedance.

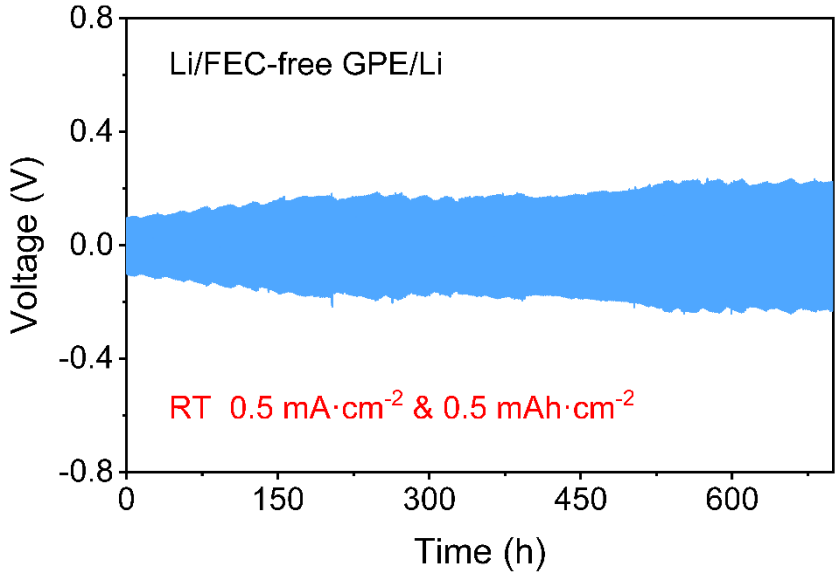

Fig. R8. Galvanostatic cycling curve of the Li/FEC-free GPE/Li cell under 0.5 mA cm^{-2} and 0.5 mAh cm^{-2}.

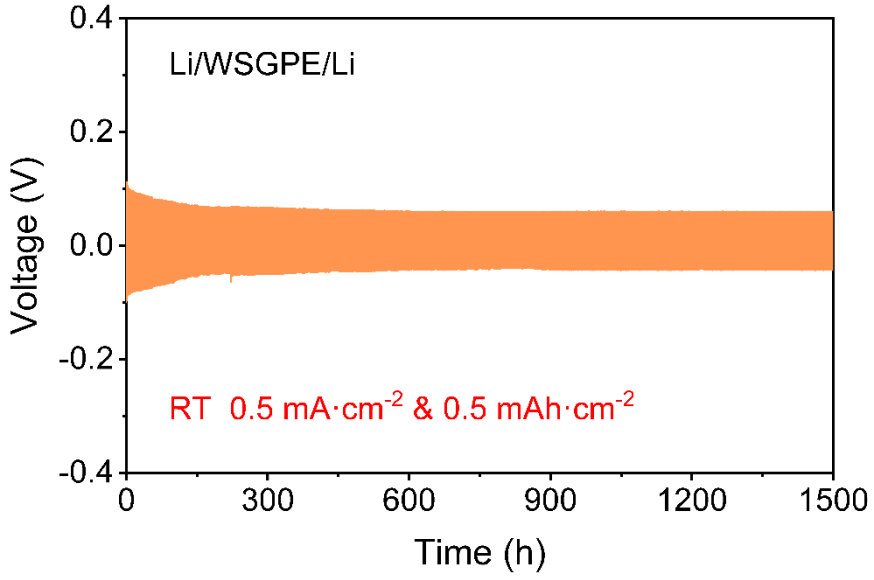

Fig. R9 (Fig. 5b in revised manuscript). Galvanostatic cycling curve of the Li/WSGPE/Li cell under 0.5 mA cm^{-2} and 0.5 mAh cm^{-2}.

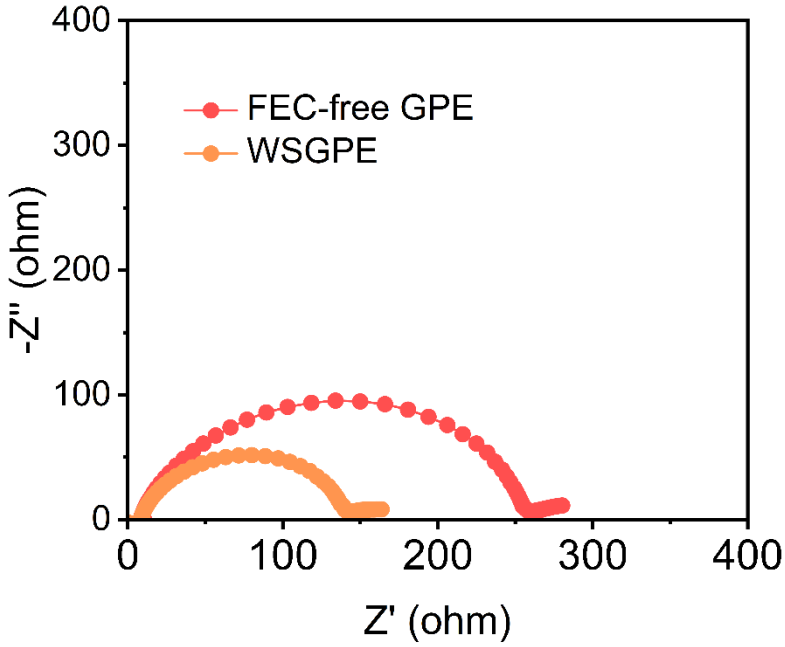

Fig. R10. EIS plots of Li symmetric cells using WSGPE and FEC-free GPE after 100 cycles.

8. Regarding FTIR discussion on Page 7: the reference sited in the manuscript employ Raman not FTIR to discuss presence of FA, CIP, and AGG.

Response: Thank you for your kind comments.

In order to make it more clearly, Raman spectra have been conducted (Fig. R11), and the relevant discussion has been provided in the revised manuscript.

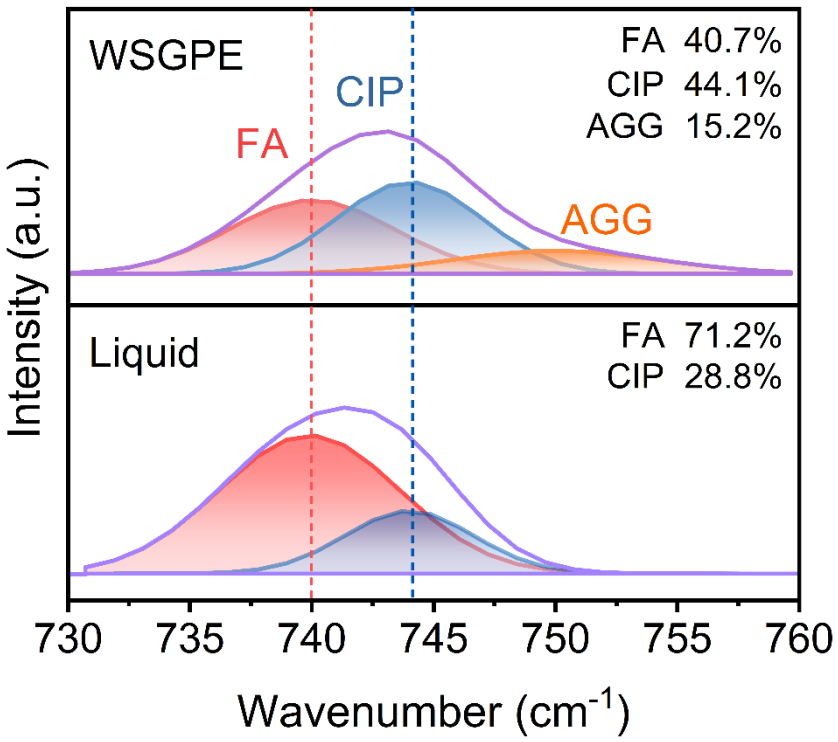

Fig. R11 (Fig. 2f in revised manuscript). Raman spectra of liquid electrolyte and WSGPE.

9. "The results from the analysis of FTIR and NMR indicate that only when FEP and PTFMA coexist, a weak solvation structure dominated by anions can be achieved (Supplementary Figs. 7-9)." However, a small but visible NMR shift from FEC based LE to FEC filled PTFMA is also observed, which indicates that a weaker solvation structure dominated by anions is formed. However, the shift is stronger for FEP probably due to the mirrored structure of PTFMA and FEP. Please rephrase.

Response: Thank you for your comments.

The slight NMR shift observed from FEC-based LE to FEC-filled PTFMA indeed indicates the generation of a weaker solvation structure. However, the FTIR results indicate that the FEP-free GPE maintains a strong solvation structure dominated by free anions (Fig. R12). Thus, it can be inferred that the weak interaction between FEC and PTFMA results in a marginally weaker solvation structure in the FEP-free GPE compared to the FEC-based LE. Nevertheless, this does not cause a transition from a

strong to a weak solvation structure. The solvation structure of the FEC-free GPE, similar to that of the FEC-based LE, is not dominated by anions. The discussion has been rephrased and yellow highlighted in the revised manuscript for clarity.

"The results from the analysis of FTIR and NMR indicate that the mirrored structure of PTFMA and FEP can effectively promote the generation of a weak solvation structure dominated by anions (Supplementary Figs. 7-9)." (Paragraph 2, Page 7)

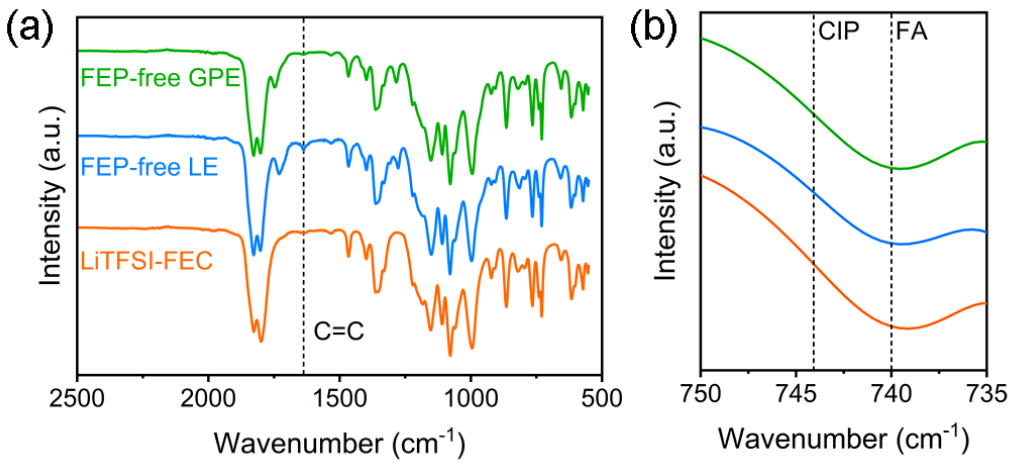

Fig. R12 (Supplementary Fig. 7 in revised Supplementary information). (a) FTIR spectra and (b) S−N−S stretching of $TFSI^-$ of FEC-based LE, FEP-free LE and FEP-free GPE, respectively.

10. The electrochemical stability window seems incorrect. In figure S10 there is an oxidation wave starting at about 4.8 V. Please revised.

Response: Thank you for your comments.

As per the references, the oxidation current density was established at 10 μA cm^{-2}, and the corresponding potential values were recorded as the oxidation potential (*Nat. Energy* 2023, 8, 1023).[4] As shown in Fig. R13, the electrochemical stability window of WSGPE is 5.05 V. We have revised the figure and text in the revised manuscript accordingly.

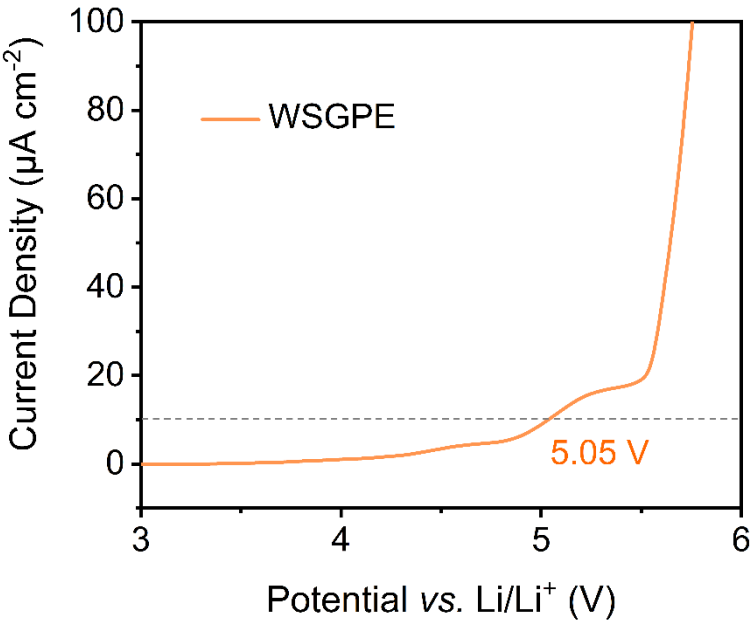

Fig. R13 (Supplementary Fig. 10 in revised Supplementary information). LSV curve of WSGPE.

11. Impedance spectroscopy in Nyquist representation must be orthonormal. Please correct all the EIS graph.

Response: We have corrected all the EIS graphs to be orthonormal.

12. Tafel plot are provided but from which type experiments and electrochemical cell? Where are the raw data to make such plots?

Response: Thank you for your comments.

Tafel plot was obtained from linear sweep voltammetry (LSV) measurement using Li symmetrical cells at a scan rate of 1 mV s^{-1}. The values of exchange current density were calculated using the Tafel equation: $\eta = a + b \log I$, where η and I are the potential and current, respectively, and a and b are constants that could be acquired after fitting the data. The raw data of the Tafel curves are shown in Fig. R14.

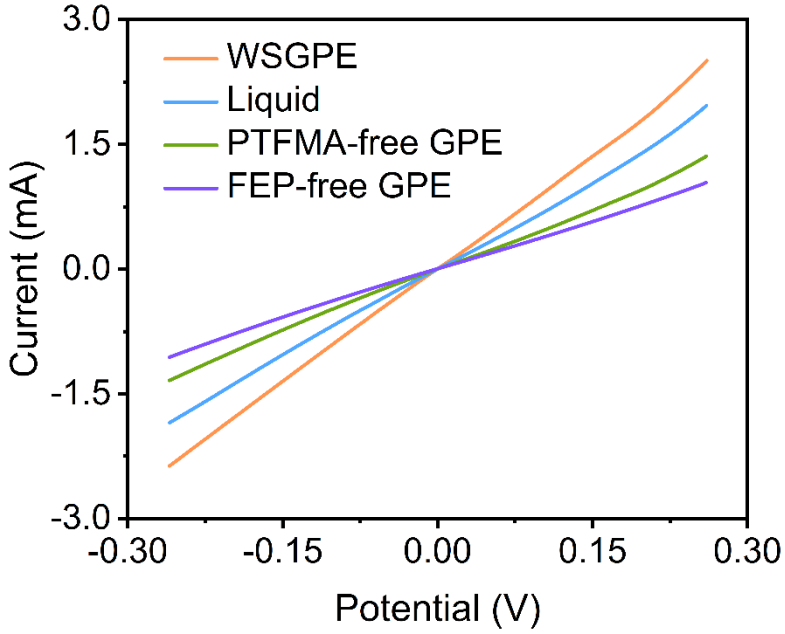

Fig. R14. LSV curves of Li symmetric cells using different electrolytes.

13. "The uniform and thin CEI not only reduces the polarization during the cycling, but also restrains the structure transition of NCM811." Can you confirm this observation by XRD? Because HRTEM is a local measurement while XRD would give you a more concreate idea of the whole instability if any.

Response: According to your comments, XRD patterns of NCM811 cathodes after 100 cycles in different electrolytes have been measured (Fig. R15). It has been reported that the evolution of the (003) peak can reflect the changes in the crystal volume of NMC811.[5] The (003) peak of NMC811 cycled in the liquid electrolyte shifted to a lower angle, indicating irreversible structural changes of NCM811. In contrast, the (003) peak of NMC811 cycled in WSGPE remains almost constant, suggesting good structural reversibility and integrity. These results have been added in the revised Supplementary information as Supplementary Fig. 35.

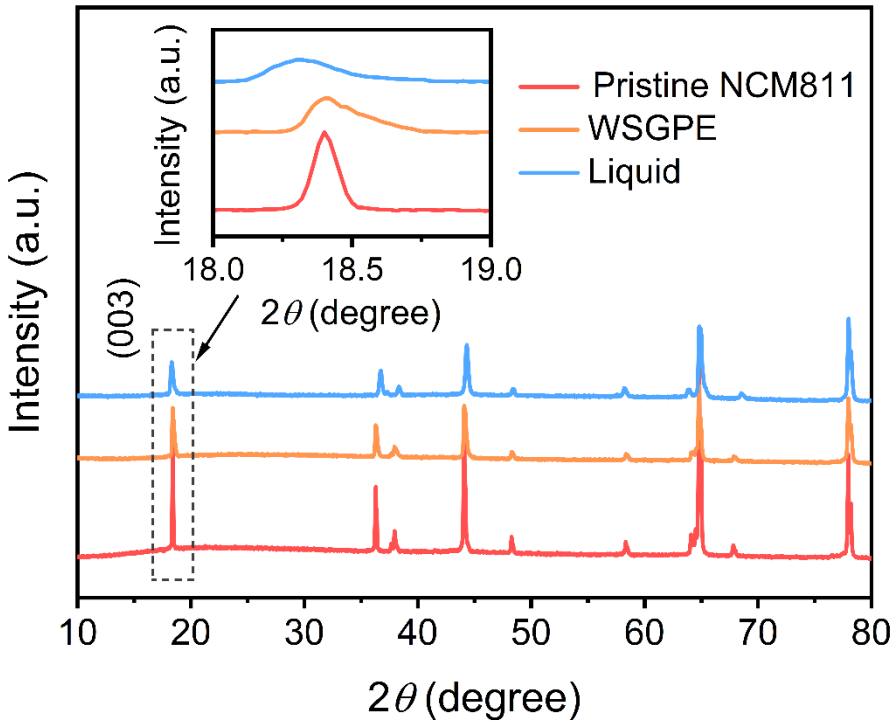

Fig. R15 (Supplementary Fig. 35 in revised Supplementary information). XRD results of pristine NMC811, NCM811 with WSGPE and liquid electrolytes after 100 cycles.

14. "The wide electrochemical window, high ionic conductivity, and Li^+ transference number make the WSPE can be used in high-voltage Li metal batteries." This sentence is grammatically wrong. Please rephrase.

Response: This sentence has been corrected and yellow highlighted in our revised manuscript.

"The wide electrochemical window, high ionic conductivity, and high Li^+ transference number make WSGPE suitable for use in high-voltage Li metal batteries." (Paragraph 4, Page 7)

15. Regarding TOF-SIMS, why depth scale is missing? How about other elements?

Response: Thank you for your kind comments.

The TOF-SIMS test provides a direct correlation between signal intensity and sputter time. Different sputtering conditions result in different sputtering rates, and

these rates can be approximated by testing standard samples. However, it's important to note that these approximations do not accurately represent the true sputter depth of the sample. Tests on standard samples yielded a sputtering rate of about 10 nm min^{-1} for a Cs^+ (2 keV, 100 nA) ion beam on SiO_2 (sputtering area of 250 μm× 250 μm). Information on the other elements is demonstrated in Fig. R16. This figure has been added as Supplementary Fig. 34 in the revised Supplementary information.

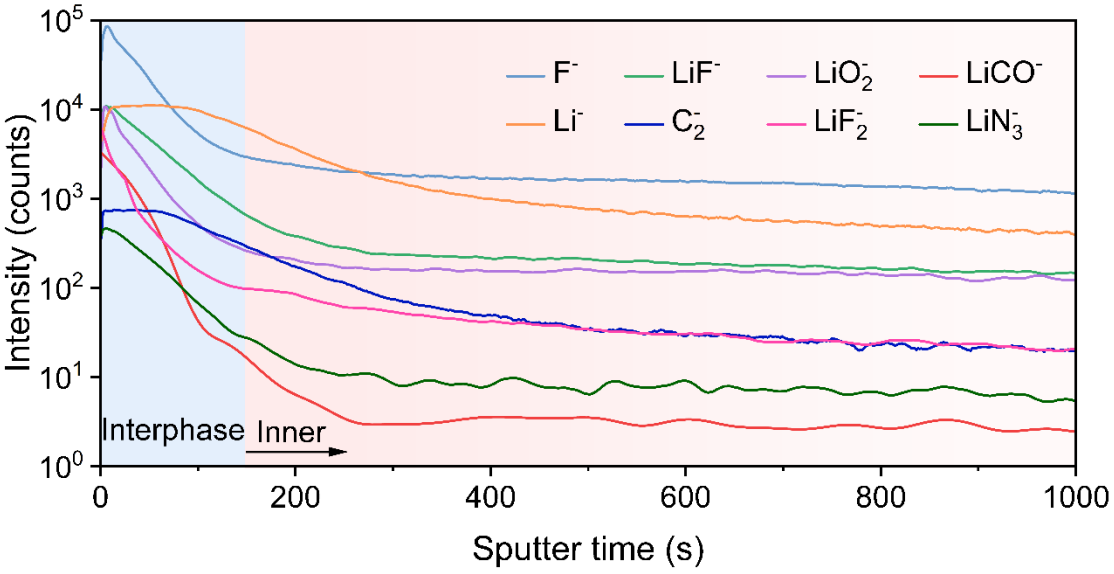

Fig. R16 (Supplementary Fig. 34 in revised Supplementary information). TOF-SIMS depth profiles for the cycled Li anode.

16. Please indicate the pressure applied during cycling if any.

Response: During cycling, the pouch cells were sandwiched in the stainless-steel clamping device with an external pressure of approximately 196 kPa.

17. Method parts: only FTIR and some electrochemical methods are provided whereas plenty of techniques are reported in this work from Raman to TOF-SIMS via NMR etc. . This is not consistent. How were samples prepared for XPS and TOF-SIMS characterizations.

Response: According to your comments, the detailed information has been added and highlighted in yellow in the Methods section of the revised manuscript.

"Fourier transform infrared (FTIR) spectra of electrolytes were collected on a

Thermo Scientific Nicolet 6700 instrument. Raman spectra were collected on a Via Renishaw Raman spectrometer system using a 532 nm wavelength laser. The precursor solution and polymer electrolyte were dissolved in Chloroform-d1 for NMR analysis on a Bruker AVANCE III 600 MHz. Flame-retardant properties were tested by combustion experiment." (Paragraph 4, Page 16)

"The cycled cells were carefully disassembled in a glovebox, and the cycled Li foils and NCM811 cathodes were washed with dimethyl carbonate (DMC, Aladdin) and dried at room temperature. The morphologies of Li anodes were observed by scanning electron microscope (SEM, Hitachi S-4800). X-ray photoelectron spectroscopy (XPS) was performed on Thermo Scientific K-Alpha. All peaks were fitted according to the reference peak of C-C bond at 284.8 eV. X-ray diffraction (XRD) was performed on the X-ray diffractonmetry (Rigaku Smartlab). A filtered Cu Kα1 (λ = 0.15406 nm) radiation source at 40 kV and 40 mA was used. XRD data were collected at room temperature in the range of 10°~80°. Time-of-flight secondary ion mass spectrometry (TOF-SIMS) was carried out on a TOF-SIMS 5 – 100 instrument (ION-TOF GmbH) equipped with Bi^{3+} as the primary ion source (30 keV) over an area of 250 μm × 250 μm. The depth profiles of TOF-SIMS were acquired on the area of 70 μm × 70 μm using Cs^{+} as the sputter source (2 keV), and the sputter rate is about 10 nm min^{-1} on SiO_2." (Paragraph 4, Page 17)

18. The reviewer spent most of their time reding the supporting info file (33 figures in it) rather than focusing on the manuscript which presents rather concept figures than experimental data.

Response: Thank you for your comments. In the revised version, we have paid more attention on delivering our design and concept supported by experimental data. To clarify, a major modification has been made on the introduction. The concept figures in the manuscript were also simplified.

Response to Reviewer #5:

I co-reviewed this manuscript with one of the reviewers who provided the listed reports.

This is part of the Nature Communications initiative to facilitate training in peer review and to provide appropriate recognition for Early Career Researchers who co-review manuscripts.

Response: Thank you for your attention and kind comments.

References

1. Zhang, X. Q. et al. Fluoroethylene carbonate additives to render uniform Li deposits in lithium metal batteries. *Adv. Funct. Mater.* **27**, 1605989 (2017).
2. He, H. et al. Effect of fluoroethylene carbonate additive on the low‐temperature performance of lithium‐ion batteries. *J. Electroanal. Chem.* **925**, 116870 (2022).
3. Li, W. et al. Deep eutectic solvent with film-forming fluoroethylene carbonate as a nonflammable electrolyte for lithium metal batteries. *J Energy Storage* **68**, 107766 (2023).
4. Meng, Y. et al. Designing phosphazene-derivative electrolyte matrices to enable high-voltage lithium metal batteries for extreme working conditions. *Nat. Energy* **8**, 1023‐1033 (2023).
5. Gong, Y. et al. Ultra-thin and high-voltage-stable Bi-phasic solid polymer electrolytes for high-energy-density Li metal batteries. *Nano Energy* **119**, 109054 (2024).